MICROWAVE-ASSISTED CATALYTIC PYROLYSIS OF REFUSE-DERIVED FUEL TO IMPROVE PYROLYSIS PERFORMANCE AND BIOCHAR PROPERTIES

by

Pu Yang

B.Eng., Tianjin University, 2017

A THESIS SUBMITTED IN PARTIAL FULFILLMENT OF

THE REQUIREMENTS FOR THE DEGREE OF

MASTER OF APPLIED SCIENCE

in

THE FACULTY OF GRADUATE AND POSTDOCTORAL STUDIES

(Chemical and Biological Engineering)

THE UNIVERSITY OF BRITISH COLUMBIA

(Vancouver)

August 2020

The following individuals certify that they have read, and recommend to the Faculty of Graduate and Postdoctoral Studies for acceptance, a thesis entitled:

Microwave-assisted Catalytic Pyrolysis of Refuse-derive Fuel to Improve Pyrolysis Performance and Biochar Properties

submitted by Pu Yang in partial fulfillment of the requirements for

the degree of Master of Applied Science

in Chemical and Biological Engineering

Examining Committee:

Xiaotao Bi, Chemical and Biological Engineering, UBC
Supervisor

Susan Baldwin, Chemical and Biological Engineering, UBC
Supervisory Committee Member

Robert Legros, Chemical Engineering, Polytechnique Montreal
Supervisory Committee Member

Abstract

Solid waste disposal and soil contamination remain severe environmental issues in many regions. Biochar can be produced via pyrolysis of solid waste and further applied for soil amendment. Microwave-assisted catalytic pyrolysis (MACP) is an innovative technology to improve pyrolysis performance and biochar quality compared with conventional pyrolysis.

This project focuses on investigating the feasibility of using MACP to produce high quality biochar from refuse-derived fuel (RDF), which is generated through pre-processing of municipal solid waste (MSW). Two main catalysts, K_2CO_3 and K_3PO_4, and their combination with bentonite and clinoptilolite, were selected to mix with RDF in a fixed bed reactor exposed to microwave radiation. By comparing heating rate and biochar properties, the optimal catalyst was identified and further evaluated under various operating conditions, i.e., microwave power input, targeted pyrolysis temperature and microwave radiation time, in order to establish the relationship between these parameters and biochar yield and properties. The produced biochar was mainly characterized by specific surface area and pore size distribution based on N_2 adsorption/desorption isotherm.

K_2CO_3 showed higher heating rate and larger specific surface area of biochar than that of K_3PO_4 due to its prominent activation effect. Synergistic effect was observed when bentonite or clinoptilolite was added into K_3PO_4 which significantly improved microwave heating rate. The optimal catalyst case was identified as 20% K_2CO_3 + 10% bentonite due to its high heating rate (163 ℃/min) and large specific surface area (206 m^2/g) of biochar. Too low a microwave power (600W) could not initiate the reaction. The optimum targeted pyrolysis temperature was determined as 500 ℃ to produce biochar with the highest specific surface area (265 m^2/g) and,

based on statistical analysis, pyrolysis temperature was the main factor that influenced biochar yield and specific surface area, followed by microwave radiation time. Biochar produced from 30 wt.% K_2CO_3 could act as a precursor of potential adsorbent, while K_3PO_4 remaining in the produced biochar could serve as essential nutrient sources for plant growth and had the potential in adsorbing and immobilizing heavy metal contents in contaminated soil.

Lay Summary

This study aims at producing high quality biochar material from a type of municipal solid waste by involving microwave heating and use of catalysts in a thermochemical process. The selected catalysts substantially accelerated the reaction and created porous structure in biochar which is quite useful for adsorption and immobilization of organic/inorganic pollutants, as well as acted as essential nutrient sources for plant growth in soil environment. Selecting suitable catalysts and reaction conditions is of great significance for producing high quality biochar. The research and development of such technologies will be beneficial for addressing the global solid waste disposal and soil amendment issues.

Preface

The research work covered in this dissertation was completed by the author, Pu Yang under the supervision of Dr. Xiaotao Bi. The author's work includes general literature review, experimental design and setup, implementation of microwave pyrolysis reactor and characterization facilities, data collection and analysis, thesis writing and revision. During the initial microwave reactor setup, the author was supported by Dr. Dening Jia. This thesis represents original, individual and unpublished work by the author. A manuscript will be prepared and submitted for publication in peer reviewed journals in the near future.

Table of Contents

Abstract ..... **iii**

Lay Summary ..... **v**

Preface ..... **vi**

Table of Contents ..... **vii**

List of Tables ..... **x**

List of Figures ..... **xii**

List of Abbreviations ..... **xv**

Acknowledgements ..... **xvii**

Chapter 1: Introduction **1**

1.1 Background 1

1.2 Literature Review 5

1.2.1 Pyrolysis of RDF 5

1.2.2 Effect of pyrolysis conditions on biochar yield and properties 7

1.2.3 Microwave-assisted catalytic pyrolysis (MACP) 8

1.2.3.1 Fundamentals of microwave heating 9

1.2.3.2 Microwave absorber and catalyst 11

1.2.3.3 Microwave pyrolysis of different feedstock to produce biochar 14

1.2.3.4 Comparisons between MACP and conventional pyrolysis 14

1.2.4 Biochar and its soil applications 15

1.3 Research objectives and tasks 17

Chapter 2: Experimental methods and setup **21**

2.1 Sample preparation 21
2.2 Experimental setup and procedures 23
2.3 Experimental design 26
2.4 Characterization 27
2.4.1 Thermogravimetric analysis 27
2.4.2 Proximate and elemental analysis 27
2.4.3 Pore properties and morphology 28
2.4.4 Functional groups 28
2.4.5 Methylene blue adsorption 29
2.5 Batch leaching test 29
2.6 Statistical analysis 30
Chapter 3: Microwave-assisted catalytic pyrolysis of RDF 31
3.1 Pyrolytic properties of RDF 31
3.2 Pyrolysis behavior of RDF in MACP 33
3.3 Effect of catalysts on heating performance of RDF 36
3.3.1 Single catalyst 36
3.3.2 Catalyst mixtures 40
3.4 Effect of microwave power intensity 43
3.5 Comparisons between RDF and sawdust 44
3.6 Summary 45
Chapter 4: Characterization of biochar 47
4.1 Effect of catalysts on biochar yield and properties 47
4.1.1 Biochar yield 47

4.1.2 Biochar compositions 50
4.1.3 Pore properties 53
4.1.4 Functional groups 60
4.2 Effect of microwave power intensity on biochar yield and pore properties 61
4.3 Effect of temperature and time on biochar yield and surface area 64
4.4 Summary 69
Chapter 5: Conclusions and future work 70
Bibliography 73
Appendices 88
Appendix A Heating performance of RDF mixed with bentonite or clinoptilolite in MACP .. 88
Appendix B Stretching and functional groups in FTIR 89
Appendix C Methylene blue adsorption test 90
Appendix D Batch leaching test 91
Appendix E Sample of descriptive and multiple comparisons of ANOVA 92

List of Tables

Table 1.1 Comparisons between conventional pyrolysis and MACP..... 15

Table 2.1 Particle size distribution of ground and pre-dried RDF sample. 22

Table 2.2 Experimental parameters investigated in MACP of RDF. 26

Table 3.1 Decomposition temperature of different components in RDF..... 32

Table 3.2 Average heating rate of pure RDF and RDF mixed with different catalysts..... 41

Table 3.3 Average heating rate of RDF mixed with 20% K_2CO_3 + 10% bentonite under different microwave power intensity. 44

Table 4.1 Compositions of pre-dried RDF, sawdust feedstock and biochar samples produced from MACP of RDF mixed with different catalysts (unit: wt.%). 51

Table 4.2 Elemental composition of original biochar samples (i.e. without catalyst separation) produced from MACP of RDF mixed with different catalysts by ICP-AES analysis..... 51

Table 4.3 Canadian Soil Quality Guidelines for agricultural soil..... 53

Table 4.4 BET surface area, average pore diameter, micropore area and pore volume of biochar produced from MACP of RDF, conventional heating of RDF (CH) and MACP of sawdust (SD) using different catalysts under 1200 W microwave power, 550 °C final temperature and 30 min microwave radiation time. 54

Table 4.5 One-way ANOVA of biochar surface area and yield under different microwave power intensity..... 63

Table 4.6 One-way ANOVA of biochar surface area and yield under different targeted pyrolysis temperature or microwave radiation time. 67

Table B.1 Functional groups and chemical bonds under related wavenumbers in FTIR. 89

Table C.1 MB adsorption of biochar samples produced from different catalysts in MACP of RDF, sawdust (SD) and conventional heating of RDF (CH) (solid to liquid ratio: 0.01 g:20 ml, concentration: 7.5*E-5 M). 90

Table D.1 Metal contents (ppm) of original biochar sample produced with different catalysts in MACP, RDF and RDF ash sample in leachates. 91

Table E.1 ANOVA descriptive table of surface area of biochar produced under different targeted pyrolysis temperature. 92

Table E.2 ANOVA multiple comparisons of surface area of biochar produced under different targeted pyrolysis temperature. 93

List of Figures

Figure 1.1 RDF process flow from CD Waste Management Ltd, UK. 2

Figure 1.2 Schematic of the pyrolysis process (Adapted from Nomanbhay et al., 2017). 6

Figure 1.3 Schematic diagram of temperature distribution, heat and mass transfer in conventional and microwave heating (Adapted from Miura et al., 2004). 11

Figure 2.1 (a) Original, (b) crushed and (c) well-mixed sample. 22

Figure 2.2 Particle size distribution of pre-dried (a) K_2CO_3, (b) K_3PO_4, (c) bentonite, (d) clinoptilolite sample. 23

Figure 2.3 Schematic diagram of the microwave unit. 24

Figure 2.4 Front view of the microwave unit. 25

Figure 3.1 TG and DTG results of pre-dried RDF sample (A) and original sawdust (B). 32

Figure 3.2 MACP stages and hotspot phenomenon. 34

Figure 3.3 Heating performance of pure RDF and RDF mixed with 10, 20 and 30 wt.% of (a) K_2CO_3 and (b) K_3PO_4 (microwave power: 1200 W). 37

Figure 3.4 Heating performance of RDF mixed with combinations of catalysts (microwave power: 1200 W). 41

Figure 3.5 Heating rates of RDF mixed with 20% K_2CO_3 + 10% bentonite under different microwave power intensity. 43

Figure 3.6 Heating rates of RDF and sawdust mixed with 20% K_2CO_3 + 10% bentonite (microwave power: 1000 W). 45

Figure 4.1 Yield of biochar produced from MACP and conventional pyrolysis of RDF and MACP of sawdust mixed with different catalysts under 1200 W microwave power, 550 °C final

temperature and 30 min microwave radiation time (%: wt.%, KP: K_3PO_4, KC: K_2CO_3, B: bentonite, C: clinoptilolite, CH: conventional heating, MH: microwave heating). 48
Figure 4.2 SEM micrographs of biochar samples produced from MACP of RDF mixed with 20 wt.% K_2CO_3, 20 wt.% K_3PO_4 and 20 wt.% K_2CO_3 +10 wt.% bentonite under 1200 W microwave power, 550 °C final temperature and 30 min microwave radiation time. 57
Figure 4.3 Pore size distribution of biochar samples produced from conventional pyrolysis of RDF, MACP of RDF and MACP of sawdust mixed with different catalysts under 1200 W microwave power, 550 °C final temperature and 30 min microwave radiation time (1 Å=0.1 nm). 58
Figure 4.4 FTIR spectra of biochar samples produced from MACP of RDF mixed with different catalysts under 1200 W microwave power, 550 °C final temperature and 30 min microwave radiation time. 60
Figure 4.5 (a) surface area and (b) yield of biochar produced by MACP of RDF mixed with 20% K_2CO_3 + 10% bentonite under different microwave power (heating rate), 550 °C final temperature and 30 min microwave radiation time. 63
Figure 4.6 (a) Specific surface area and (b) yield of biochar produced by MACP of RDF mixed with 20% K_2CO_3 + 10% bentonite under 1000 W microwave power, different targeted pyrolysis temperature (microwave radiation time: 30 min) or microwave radiation time (pyrolysis temperature: 500 ºC). 64
Figure 4.7 SEM micrographs of biochar samples produced from MACP of RDF mixed with 20% K_2CO_3 + 10% bentonite under 1000 W microwave power with different pyrolysis temperature and microwave radiation time. 68

Figure A.1 Heating performance of pure RDF and RDF mixed with 30 wt.% bentonite or clinoptilolite in MACP..... 88
Figure C.1 MB adsorption of biochar sample produced from different catalysts in MACP of RDF at different solid to liquid ratios (MB solution volume: 20 ml, concentration: 7.5*E-5 M). 90

List of Abbreviations

AC	Activated carbon
ANOVA	Analysis of variance
BET	Brunauer-Emmet-Teller
BJH	Barrett-Joyner-Halenda
CCME	Canadian Council of Ministers of the Environment
CEC	Cation exchange capacity
DTG	Differential thermogravimetry
FTIR	Fourier transform infrared spectroscopy
HDPE	High-density polyethylene
HF	Hydrogen fluoride
HSD	Honestly significant difference
ICP-AES	Inductively coupled plasma atomic emission spectroscopy
ID	Inner diameter
KC	K_2CO_3
KP	K_3PO_4
LDPE	Low-density polyethylene
MACP	Microwave-assisted catalytic pyrolysis
MB	Methylene blue
MDF	Medium density fiberboard
MSW	Municipal solid waste
OD	Outer diameter
PET	Polyethylene terephthalate

PIC	Peripheral interface controller
PS	Polystyrene
PSD	Particle size distribution
PVC	Polyvinyl chloride
RDF	Refuse-derived fuel
SEM	Scanning electron microscopy
TCLP	Toxicity Characteristic Leaching Procedure
TGA	Thermogravimetric analysis

Acknowledgements

I would like to give my sincere gratitude to my supervisor, Dr. Xiaotao Bi for his guidance, patience, kindness and encouragement on my research and course learning in this master program. I am very appreciated for his time and effort on the assistance of conducting my research. He is willing to share everything he knows which is very helpful to my study and life. I also want to thank Dr. Robert Legros and Dr. Susan Baldwin for their willingness to serve as my committee members and their useful suggestions on my experiment and thesis.

I am grateful to Nanjing Gongda Environmental Technology Co. Ltd for providing a scholarship to support my graduate study and to Dr. Yanhua Xu for his concern and help. I would also like to thank the host of the 1st International Conference on Energy and Environment for offering me an opportunity to present my results and connect with experts and peers in this research area.

I offer enduring thanks to my colleagues in the microwave pyrolysis group and workshop staff for their theoretical and technical support, respectively. I owe particular thanks to Dr. Dening Jia and Bill Cheng who gave me valuable support, and one of my lab mates, Bingcheng Lin for his assistance. I still remember those days full of hardness and happiness when we worked in the lab. I appreciate all the company and help from my friends especially during those challenging days.

Last but not least, my special thanks are given to my family, especially my parents who have supported me throughout my years of growth both morally and financially, as well as my wife who always stands by my side and makes our progress. I appreciate their timeless and priceless love, trust and support from my heart and soul.

To my beloved family

Chapter 1: Introduction

1.1 Background

With the industry booming and population growth around the world, large amounts of solid waste in various forms are generated every day, including industrial, commercial and municipal solid waste (MSW). Currently, it is estimated that 2.0 billion tons of MSW are produced annually worldwide, and it will rapidly increase to 2.2 billion tons by 2025 and 3.40 billion tons by 2050 (Chhabra et al., 2016; Ellis, 2018). With increasing concerns, solid waste disposal has become an intractable and urgent problem in many countries and regions, especially in South and East Asia. Depending on the properties, some solid waste has been recycled (~13.5%) or composted (~5.5%), whereas most have been landfilled or burned which causes ecological and environmental issues. Different methods have been under exploration to alleviate the burden of managing and disposing solid waste or to utilize them to produce energy and products, following the so-called waste-to-energy strategy. One approach is to apply thermochemical technologies to not only eradicate solid waste residues, but also produce heat, electricity or value-added products. The combustible fractions of solid waste could be extracted through step-by-step physical pretreatments, including crushing, screening, classifying (recycling inert materials such as glass and metal) and pelletizing, and made into a densified solid fuel — refuse-derived fuel (RDF). Generally, RDF is composed of waste plastics, paper, wood and fiber scraps. It has a higher heating value, more uniform size and composition, more stable properties and is thus much easier to be stored and transported than original solid waste such as MSW. For thermochemical conversion such as combustion or gasification, RDF could overcome the disadvantages of MSW on inconsistent energy content and non-uniform heating of heterogenous solid waste (Belgiorno et al., 2003).

Refuse-derived fuel (RDF) is a fuel processed from various types of waste, such as MSW, industrial or commercial waste. In general, the composition of RDF includes combustible non-recyclable plastics, paper cardboard, labels and other corrugated materials and it varies among different regions and processing technologies. As is shown in Figure 1.1, the process aims to remove inert materials, reduce particle size and shape amorphous waste so that RDF could become an energy source with recoverable calorific value. It is popular among Japan and European countries where plenty of RDF from bulk MSW is produced daily due to their territory restrictions. The most common application of RDF is to substitute a portion of fossil fuels in a rotary cement kiln (Ozkan and Banar, 2010). It can also be burned in power plants to produce electricity (Longo et al., 2020). However, the calorific value of RDF is low at 8-14 MJ/kg, which results in low heat generation in combustion applications. With the rapid increase in the amount of produced RDF, other potential applications for producing value-added products from RDF are encouraged.

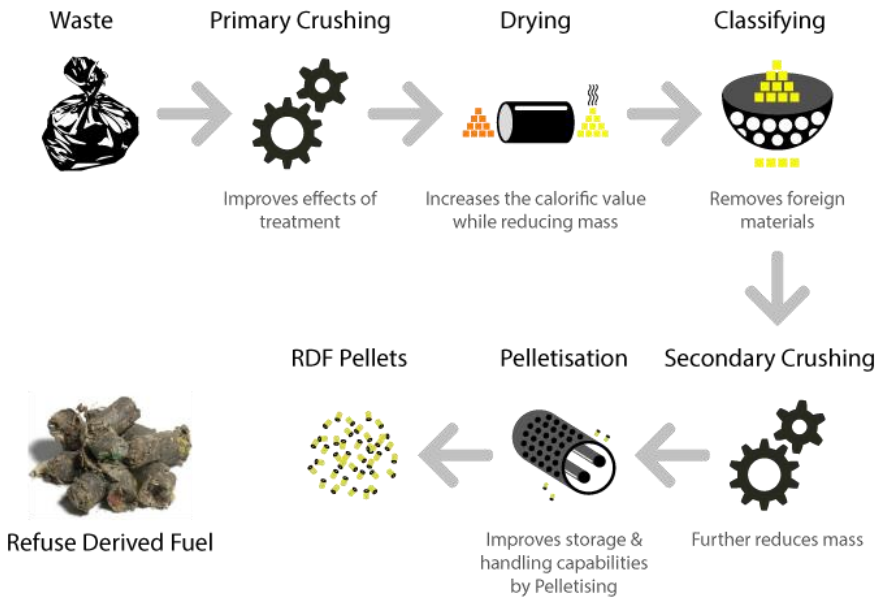

Figure 1.1 RDF process flow from CD Waste Management Ltd, UK.

Pyrolysis is a thermal decomposition reaction at a temperature range of 400-600 °C and a short residence time (< 600 s) which transforms the feedstock into the products including non-condensable gases (e.g. CO, H_2, CH_4), bio-oil (hydrocarbons and oxygenated compounds) and biochar (Bridgwater, 2012; Mohamed, 2018). As a byproduct, biochar is a dark solid charcoal with porous structure and has various potential applications, especially as an adsorbent for soil amendment (Chun et al., 2004). Aiming at producing biochar with high specific surface area and large pore volume to adsorb and stabilize organic pollutants and heavy metals, high heating rate is usually required to reach pyrolysis temperature and maintain for enough reaction time (Mohamed et al., 2016a; Veksha et al., 2014). Although slow pyrolysis can achieve more carbonization and thus high solid yield, it is relatively difficult to produce high quality biochar because of its low heating rate (Manyà et al., 2015).

Fast pyrolysis has been used to produce biochar of good physicochemical properties and pore structure (Efika et al., 2015; Mullen et al., 2010). Pyrolysis with rapid heating and at high temperature could trigger the destruction of lignocellulosic structures to create abundant porosity in biochar (Zhang et al., 2015). For most of the conventional pyrolysis performed in electrically heated fixed bed reactors, slow heating is expected to occur mainly due to the limitations of heat transfer between feedstock particles. Due to the unique heating characteristics of microwave, the integration of microwave heating for catalytic pyrolysis is an innovative concept to achieve fast pyrolysis of biomass in different forms and compositions to produce high quality bio-oil and biochar. Various types of biomass feedstock have been examined in microwave pyrolysis to generate desired products. However, due to the poor microwave absorption of dry biomass, catalysts or microwave absorbers need to be added in-situ to increase microwave absorption rate,

so as to reach desired pyrolysis temperature at lower microwave power. Microwave-assisted catalytic pyrolysis (MACP) appears to be a promising technology to convert RDF into useful biochar products if proper catalyst(s) can be selected to promote microwave absorption and catalytic effects to create more porous structures in biochar.

Heavy industrial and agricultural activities have resulted in soil degradation and contamination. One serious problem is soil pollution by heavy metals (e.g., Pb, Cr, Cd, Cu, Zn, etc.) which lowers the crop yield and soil fertility. Notably, contaminated soil becomes a non-neglected threat to human health through food chain, as these heavy metal ions may leach out into ground water system and accumulated in the plant matrix (Ahmad et al., 2014; Puga et al., 2015). Therefore, soil amendment and remediation have attracted more and more attention in addressing environmental health. Biochar of large specific surface area, large volume of pore structures and varieties of oxygenated functional groups have the ability to adsorb and immobilize heavy metals (Cao et al., 2019; Inyang et al., 2016; Wang et al., 2017). Some compounds such as phosphate are well known as not only the nutrient source for plants, but also an excellent immobilizer to form a stable compound with heavy metals, especially Pb^{2+} (Bolan et al., 2014a). Those compounds may serve as catalysts in MACP, and also act as heavy metal immobilization and fertility improvement when applied with biochar.

In this study, MACP of RDF is applied to investigate the feasibility on improving heating performance and producing high quality biochar for soil applications. Four catalysts (K_3PO_4, K_2CO_3, bentonite and clinoptilolite) and their mixtures with RDF at different loadings are applied in MACP to identify and compare the effectiveness on accelerating microwave heating and

creating porous structures and useful functional groups for adsorption in biochar. It should be emphasized that the high specific surface area of biochar is the main target of this research and the optimum operating conditions (i.e., microwave power input, targeted pyrolysis temperature and microwave radiation time) are thus investigated and determined on producing biochar with the highest surface area for each given catalyst. All biochars are produced in a one-step pyrolysis process without further activation.

1.2 Literature Review

1.2.1 Pyrolysis of RDF

Pyrolysis is a thermochemical decomposition reaction of organic materials at high temperatures and in an oxygen-free atmosphere. Figure 1.2 indicates two stages in pyrolysis (Nomanbhay et al., 2017). The biomass feedstock first breaks down to vapors and char with depolymerization and fragmentation in the primary decomposition stage. The vapors, also named tars, will break down or reconstruct further into non-condensable gases and liquid bio-oil, which happens in the gas phase secondary tar-cracking stage (Dmitry, 2011). Therefore, three different products are generated at the end: bio-oil, biogas and biochar, and their yields and properties depend on feedstock composition and pyrolysis conditions, such as heating rate, temperature and residence time. The typical temperature range for pyrolysis is between 350 ℃ and 600 ℃, and it requires a stable energy source to heat the feedstock continuously to reach high temperature and maintain for specific residence time. Thus, the electrically heated fixed bed reactor is typically employed to study pyrolysis in the laboratory. However, other heating methods have been developed to heat up samples quickly, such as fluidized bed reactors, cyclonic reactors, induction-heated and microwave-heated reactors.

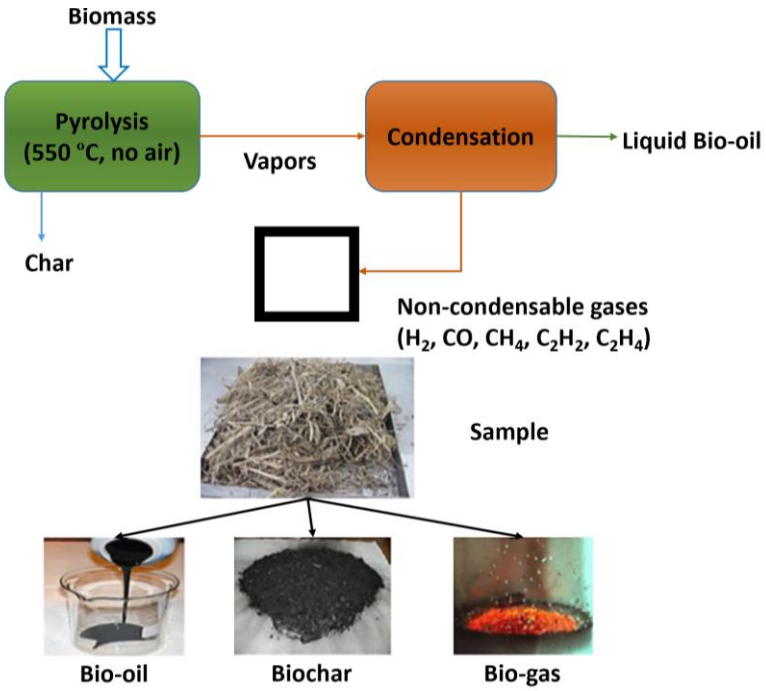

Figure 1.2 Schematic of the pyrolysis process (Adapted from Nomanbhay et al., 2017).

RDF can be pyrolyzed to generate desired products. The pyrolysis study of RDF in Italy was carried out by Cozzani et al (1995), who found that the char yield was around 23% and the biochar specific surface area was about 50 m^2/g at a pyrolysis temperature well above 500 °C. Paper cardboard, waste plastics and woody materials were regarded as three key components of RDF, which determine the thermal behavior of bulk RDF during pyrolysis (Cozzani et al., 1995a). Silva et al. (2015) investigated the pyrolysis of RDF components (nonpackaging paper, textile, polyethylene film, packaging polypropylene wastes, etc.) and found that the RDF derived char resembles mostly that of the biochar derived from nonpackaging paper waste(Silva et al., 2015)(Silva et al., 2015). Bio-oil and syngas produced from pyrolysis of RDF were also investigated. Bio-oil derived from slow pyrolysis contained more oxygenates, alkanes and alkenes, whereas fast pyrolysis of RDF produced more aromatics (Efika et al., 2015). Khongkrapan et al. (2014) applied microwave plasma assisted pyrolysis of RDF and reported that the gas yield was in

the range of 1.0-1.7 m^3/kg, containing 14% H_2, 66% CO and 4% CH_4, with a heating value of 11 MJ/m^3. In conclusion, instead of combustion, pyrolysis is a feasible pathway to utilize RDF to produce value-added bio-oil and syngas. However, the RDF derived biochar has a low yield and poor quality.

The main compositions of RDF are cellulose, hemicellulose, lignin and polymers (plastics) which decompose and depolymerize to form various types of small molecules, including light hydrocarbons and gases (CO, H_2, CO_2, etc.) in different temperature ranges during pyrolysis. The decomposition of cellulose involves dehydration, decarboxylation, carbonylation and depolymerization, in which decarboxylation and carbonylation produce more biochar and gases (Basu, 2013). Hemicellulose is more reactive as its decomposition temperature (~250 °C) is lower than cellulose (~350 °C) (Bridgwater, 2012; de Wild et al., 2009). The decomposition of lignin occurs within a wide temperature range (200-600 °C) and is the most difficult because of the existence of stable bonds in aromatic rings in carbon skeleton. However, it is expected to give the highest solid yield (~50 %) (Zhao et al., 2017). The degradation of polymers usually occurs around 450 °C and favors the production of tar vapors and liquid bio-oil (Arshad et al., 2017). With the decomposition and devolatilization of different components, various channels are created in the biochar matrix, thus increasing specific surface area and pore volume (Liu et al., 2012; Lu, 1994).

1.2.2 Effect of pyrolysis conditions on biochar yield and properties

Pyrolysis conditions, i.e., heating rate, pyrolysis temperature and residence time, could also have a great impact on biochar yield and properties. Zhao et al. (2018) investigated the effect of those parameters on rapeseed stem derived biochar and found that pyrolysis temperature had the most

significant impact on biochar properties and demonstrated a positive relationship with pH, microporous structure, specific surface area, fixed carbon and ash content, and a negative correlation with yield, average pore size, number and density of functional groups, volatile matter and total H and O content (Zhao et al., 2018). Especially for pore properties, Liew et al. (2018) found that the BET surface area of biochar produced from microwave pyrolysis of oil palm waste increased from 80 m^2/g to 210 m^2/g with increasing microwave power input from 500W to 700W (Liew et al., 2018). However, it should be noted that the positive relationship between temperature and specific surface area is only a general trend, as some researchers also reported that the specific surface area decreased with increasing temperature above 600 °C due to the fusion of pores (Chun et al., 2004; Kumar et al., 2017). Similar phenomena could be found at too high a microwave power and too long a residence time (Foo and Hameed, 2012a; Zhang et al., 2015). On the other hand, pyrolysis temperature showed a strong negative correlation with biochar yield (Baçaoui et al., 2001; Villota et al., 2018; Zhang et al., 2016). The variation of residence time between 10 and 100 mins showed less effect on biochar yield, whereas the heating rate had the least influence on biochar yield (Ahmad et al., 2014; Zhao et al., 2018). As a result, it is of great significance to investigate the optimal operating condition on producing biochar with the highest specific surface area and yield in pyrolysis of RDF.

1.2.3 Microwave-assisted catalytic pyrolysis (MACP)

In recent decades, microwave-assisted catalytic pyrolysis (MACP) has been proposed as a novel approach to combine microwave radiation with catalysts as a microwave receptor and activator to alter the biomass pyrolysis process. Many types of biomass have been examined in MACP, such as sawdust (Park et al., 2010), corn stover (Mullen et al., 2010), wheat straw (Zhao et al., 2014),

macroalgae (Zhang et al., 2016), sewage sludge (Domínguez et al., 2006), etc. When dealing with dry biomass with poor microwave absorption, adding suitable microwave absorbents are very important to reach targeted temperature and to upgrade biochar. Various types of microwave absorbers or catalysts can be used, such as inorganic reagents (NaOH, HCl, NH_4Cl, etc.), inorganic compounds (Al_2O_3, Fe_3O_4, K_3PO_4, etc.), natural zeolites and clays (dolomites, bentonite, clinoptilolite, etc.) and conductive materials (SiC, char, graphite, etc.) (Menéndez et al., 2010; Mohamed et al., 2016b; Shang et al., 2015). Those catalysts may give different results on the yield and properties of biochar.

1.2.3.1 Fundamentals of microwave heating

Microwave refers to the wavelength from 1 mm to 1 m and corresponding frequency range of 0.3-300 GHz on the electromagnetic spectrum. In domestic and industrial applications, the commonly used frequencies are 0.915 and 2.45 GHz. According to the response to microwave, materials could be classified into three types: conductors (microwave passes through without energy level drop), insulators (microwave is reflected or blocked) and absorbers (microwave is absorbed and converted to other forms of energy). Microwave absorbers are also called dielectrics, as their ability to absorb microwave is determined by their dielectric properties, including dielectric constant and dielectric loss.

Generally, the heating mechanism of microwave can be elucidated in two aspects: dipolar and interfacial (Maxwell-Wagner) polarization. The former accounts for polar molecules, whereas the latter specifically refers to materials with free charges. The permanent and temporarily induced dipoles in polar molecules (e.g. H_2O) rotate to be aligned to the alternating electromagnetic field

and results in the energy dissipation as heat from intrinsic resistance to the rotation movements (friction) of dipoles (Menéndez et al., 2010). Their ability to be aligned to the field through rotation defines its dielectric properties. On the other hand, interfacial polarization exists between materials with varied dielectric properties or in solid materials with free charges, such as π-electrons in carbon material (Zlotorzynski, 1995). Free charges are displaced from the equilibrium point which results in polarization. Once the polar molecule is unable to follow the oscillation of the field, they become out of phase, leading to accumulation of charges and dissipation of heat because of the Maxell-Wagner effect (Zlotorzynski, 1995). The lag between dipole phases and the field is called relaxation time τ, where the maximum microwave absorption rate happens at the frequency of $f=1/\tau$ (Pütun et al., 2009). This difference defines the dielectric loss tangent, $\tan\delta=\varepsilon''/\varepsilon'$, in which ε'' is the dielectric loss factor, indicating the amount of heat converted from electromagnetic energy, and ε' is the dielectric constant factor, determining the ability of molecules to be polarized by the field (absorb microwave energy).

The unique characteristics of microwave heating include rapid, volumetric and selective heating (Arshad et al., 2017; Huang et al., 2016; Metaxas and Meredith, 2011). As shown in Figure 1.3 (Miura et al., 2004), heat is transferred from outer surface to the interior region of particles through conduction and convection in conventional heating. It requires better heat transfer and enough contact time to achieve an efficient heating and uniform temperature distribution. On the contrary, microwave heating is defined as the conversion of electromagnetic energy to heat. Microwave penetrates directly into the particle where adsorbed microwave energy is released as heat volumetrically throughout the layers of the bulk material (Nomanbhay et al., 2017). Therefore, all regions are heated simultaneously in an efficient way. Meanwhile, microwave is absorbed by

molecules with better dielectric properties. For multi-phase material with different dielectric properties, only specific compositions are heated with varied temperature distribution, which reduces separation pretreatments if only specific components in the feedstock are expected to be heated up (Dernovsek et al., 2001).

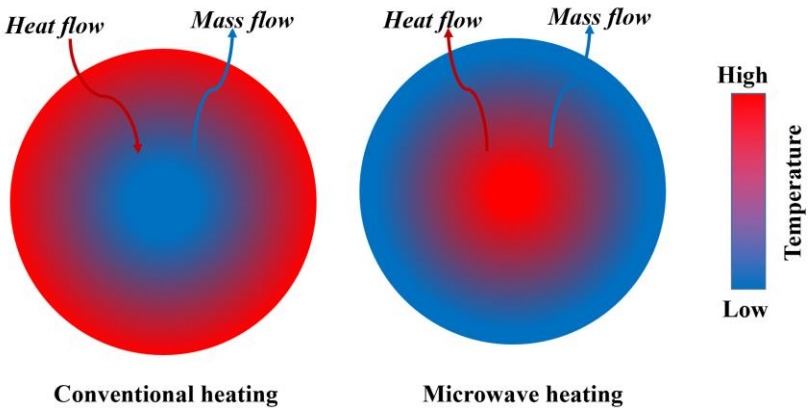

Figure 1.3 Schematic diagram of temperature distribution, heat and mass transfer in conventional and microwave heating (Adapted from Miura et al., 2004).

1.2.3.2 Microwave absorber and catalyst

To improve the microwave absorption and heating rate during pyrolysis, as well as biochar properties, different microwave absorbers or catalysts have been explored to identify their effectiveness. The general selection criteria of suitable catalysts include good dielectric properties for microwave absorption and conversion to heat, and strong catalytic effect on thermo-cracking and biochar pore creation. For soil applications of biochars, the catalyst should also be non-toxic and economic, better containing plant nutrients.

It was reported that K_2CO_3 is a very effective activator to improve pore properties and strengthen aromatic structures of biochar. Haeldermans et al. (2019) reported that biochar was more carbonized and aromatized when adding no less than 5 wt.% K_2CO_3 in microwave-assisted

pyrolysis of medium density fiberboard (MDF), due to the strong catalytic effect of K_2CO_3 under high temperature. Foo and Hameed (2011) focused on the preparation of activated carbon (AC) using K_2CO_3 and KOH in microwave induced activation of fruit peels and rice husks. K_2CO_3 activated sample showed higher yield, better pore structures and adsorption capacity than KOH activated sample, with BET surface area, total pore volume and monolayer adsorption capacity of 1165 m^2/g, 0.78 cm^3/g and 44.15%, respectively, in microwave induced activation of rice husks. Similar results were reported in other studies (Foo and Hameed, 2012b, 2012c; Nowicki et al., 2016; Okman et al., 2014). Deng et al. (2010) found that K_2CO_3 produced more mesopores in AC than KOH in microwave-assisted activation of cotton stalk. In addition to K_2CO_3, other additives such as SiC, coke and pyrolysis char, have also been applied in MACP (Shang et al., 2015). However, they mainly serve as microwave absorbers without little catalytic effect.

Potassium plays an important role on reducing the decomposition temperature and increasing the yield of solid, gas and phenol compounds (Trendewicz et al., 2015; Zhang et al., 2017). Chemical reactions such as dehydration and demethoxylation are also favored by potassium which lead to higher solid yield (Di Blasi et al., 2017; Hwang et al., 2013). Meanwhile, phosphorus has similar effects on decreasing decomposition temperature and promoting char formation. Both potassium and phosphorus were found to catalyze the decomposition of cellulose and hemicellulose and increase char yields, but lowering bio-oil yield in fast pyrolysis of beech wood (Banks et al., 2016). K_3PO_4 has shown a noticeable effect on increasing microwave heating rate and improving biochar quality for further activations of AC (Lu et al., 2018; Mohamed, 2018).

Considering the very poor dielectric properties of RDF that contains large portions of waste plastics which are transparent to microwave, the selected catalyst should absorb enough microwave and convert it into heat, which is the prerequisite for MACP of RDF. On the other hand, K and P elements remaining in the biochar-catalyst mixtures could serve as essential nutrients for plants when biochar is applied to soil. Phosphate is also a promising compound to act as a heavy metal adsorber and immobilizer for treating contaminated soil (Miretzky and Fernandez-Cirelli, 2008; Osborne et al., 2015). Thus, K_2CO_3 and K_3PO_4 are chosen as main catalysts in this study.

Natural clays (bentonite, dolomites, kaolin, etc.) and zeolites (Y-zeolite, ZSM-5, clinoptilolite, etc.) as an additive have also been investigated (He et al., 2010; Mohamed et al., 2016a; Park et al., 1999; Sulman et al., 2009). Zeolites showed an excellent effect in cracking the secondary tar cracking reactions and producing more aromatics and hydrocarbons (Miandad et al., 2017). Among them, bentonite and clinoptilolite possess a better heat transfer between solids and good adsorption performance due to their unique structure. Clinoptilolite is suitable for producing light olefins by its catalytic cracking effect, whereas bentonite demonstrates well-known effect on plant growth and soil applications, such as detoxifying heavy metals and promoting cation exchange (Gates et al., 2009; Pütun et al., 2009). Compared with pure inorganic compounds, they are also abundant and low cost. Consequently, bentonite and clinoptilolite might be promising secondary additives to combine with main catalysts to improve microwave heating performance and biochar quality, as well as to extend the soil applications of biochar. The synergistic effects of dual catalysts are also worth to be investigated.

1.2.3.3 Microwave pyrolysis of different feedstock to produce biochar

With the assistance of microwave absorbers or catalysts, different dry biomass feedstock with poor dielectric properties can be pyrolyzed in MACP to examine the effect of feedstock composition on the yield and properties of biochar. Over the past years, researchers have been investigating various biomass feedstock for producing biochar with high specific surface area and useful functional groups. These biomass feedstocks can be classified into woody biomass (wood chips, sawdust, etc.), herbaceous biomass (switchgrass, wheat straws, bamboo, etc.), solid waste and sewage sludge. It was found that microwave pyrolysis of biomass could produce biochar with a yield ranging from 2 to 61 wt.% and BET surface area up to 800 m^2/g (Li et al., 2016). Wood blocks were tested in rapid pyrolysis with microwave heating and the produced biochar had a larger surface area (450 m^2/g) than conventional pyrolysis (184 m^2/g), but the char yield was low (< 20%) (Miura et al., 2004). The specific surface area of biochar produced from MACP of switchgrass mixed with K_3PO_4 was 76.3 m^2/g, much higher than biochar produced via conventional pyrolysis (0.33 m^2/g) (Mohamed et al., 2016b). The biochar derived from microwave pyrolysis of sewage sludge showed a low specific surface area, probably due to the high ash content of sewage sludge and may be difficult for soil applications because of heavy metals originally contained in the feedstock (Karayildirim et al., 2006; Wang et al., 2020). However, there has been little research on microwave pyrolysis of municipal solid waste to generate biochar and no previous work on MACP of RDF.

1.2.3.4 Comparisons between MACP and conventional pyrolysis

MACP has many advantages over conventional pyrolysis, especially in view of the high heating efficiency and product quality. However, problems and challenges still exist. The primary concern

is the high cost, including the energy consumption, maintenance of microwave reactor, recycle of proper catalysts and absorbers (Yin, 2012). Other challenges include the poor reproducibility of product yield and quality due to the inhomogeneity of microwave field (Huang et al., 2016). Comparisons between conventional pyrolysis and MACP are given in Table 1.1 (Huang et al., 2016; Ingole et al., 2016; Luque et al., 2012; Mushtaq et al., 2014).

Table 1.1 Comparisons between conventional pyrolysis and MACP.

	Conventional pyrolysis	MACP
Advantages	Flexibility of feedstock	High heating rate and product quality
	Mature design and operation	Uniform and targeted heating
Disadvantages	Inefficient processing	Difficulty in temperature measurement
	Low product quality	High cost
	Non-selective heating	Inhomogeneity of products

In order to improve biochar quality, MACP could be used as a promising way to create more porous structure particularly due to the uniform release of volatiles throughout the whole particle (Miura et al., 2004). The produced biochar with better pore properties could act as adsorbents directly or as suitable precursors for further activation to activated carbon with better adsorptive capacities.

1.2.4 Biochar and its soil applications

Biochar is a dark and stable solid by-product with high carbon content obtained from pyrolysis of biomass (Tripathi et al., 2016). The structure of biochar is predominantly amorphous but contains some local crystalline structure of conjugated aromatic compounds and graphite-like non-aligned layers (Xiao et al., 2018). Pores of different sizes exist in the biochar matrix resulting from the

cracking of original biomass structures. The carbon atoms in biochar are strongly bound to each other, causing them to be resistant to the decomposition by microorganisms (Farrell et al., 2013). The main applications of biochar are for soil amendment and as a fertilizer, as well as for carbon sequestration. The physicochemical characteristics of biochar include density, pH, elemental composition, specific surface area and pore volume, functional groups, cation exchange capacity (CEC) and water holding capacity (WHC), etc. These parameters are mainly influenced by feedstock compositions, particle size and operating conditions in conventional pyrolysis (Li et al., 2016). As a result, biochar can be tailored with desired physicochemical properties to meet specific applications.

For soil amendment, biochar adsorbs and immobilizes organic compounds and heavy metals in contaminated soils. The physicochemical adsorption capacity is determined by specific surface area, pore volume and functional groups. It is believed that the physical adsorption depends on the diffusion rate of heavy metal ions into the pores and the number of active sites, whilst the chemical adsorption is determined by the chemical bonding between oxygenated functional groups and metal ions (Barton, 1987; Fahmi et al., 2018; Wang et al., 2017). The adsorption capability of biochar on heavy metal ions can be attributed to the co-effects of physical and chemical adsorption, as well as ion exchange capacities (Wang et al., 2017).

Only the adsorption of pollutants and heavy metals in soil is not enough for plant growth, it also requires the stable supply of essential nutrients. This is the advantage of biochar over other natural or synthetic soil amendments such as cattle manure (to reduce Cr) and green rusts (mixture of Fe^{2+} and Fe^{3+} hydroxides to reduce Hg) (Bolan et al., 2014b). Biochar has demonstrated high CEC to

hold both nutrients and soil contaminants. In a column leaching test, biochar derived from pepperwood at 600 °C reduced the total amount of nitrate, ammonium and phosphate nutrients in the leachates by 34.0%, 34.7% and 20.6%, respectively (Yao et al., 2012). In another experiment on the bioavailability and heavy metal leaching, it was found that the amount of extractable and leachable Cd and Pb in synthetic rain water substantially decreased with the application of the empty fruit bunch derived biochar (Fahmi et al., 2018). Thus, biochar plays an important role in reducing toxicity and improving soil fertility.

Biochar yield directly determines the cost and efficiency of industrial scale-up production. It is predominantly dependent on the fixed carbon content in the feedstock. The operating conditions have some impacts on biochar yield as well. To maximize biochar yield, slow heating rate and low pyrolysis temperature are favored, which, however, produces biochars of poor pore properties. Consequently, the heating rate and pyrolysis temperature need to be optimized to achieve a high yield of high quality biochar in MACP of RDF.

1.3 Research objectives and tasks

RDF is a solid fuel derived from MSW, which has been commonly used as a fuel substitute for the cement kiln. Meanwhile, conventional pyrolysis of RDF has been researched in the laboratory units to produce bio-oil and syngas, but challenged by poor heating performance and product quality. The feasibility of pyrolysis of RDF to produce high quality biochar has not been explored. The MACP of different forest and agricultural biomass feedstock showed better biochar quality than that of conventional pyrolysis due to the unique characteristics of microwave heating. Various microwave absorbers or catalysts, including inorganic compounds, zeolites, natural clays etc., have

been examined in MACP to improve microwave absorption rate and catalytic effect to improve bio-oil and biochar quality. K_2CO_3 has been applied in in-situ catalytic pyrolysis or biochar activation to produce biochar or activated carbon of high specific surface area. K_3PO_4 is a good microwave absorber, containing essential nutrients for plants and being able to stabilize heavy metals. Bentonite and clinoptilolite are good heat transfer media and can promote cracking reactions. However, it is unclear whether those catalysts can increase microwave absorption and improve biochar quality in MACP of RDF, as the composition of RDF varies significantly compared to woody biomass. Meanwhile, the pyrolysis conditions (controlled by operating parameters) may also impact on biochar yield and properties based on previous pyrolysis tests of woody biomass. The optimal operating conditions on MACP of RDF to produce high quality biochar thus still need to be identified. Conventional woody biomass derived biochar has been effective for soil amendment and prevention of heavy metal and nutrients leaching. However, there are still uncertainties on the applicability of RDF derived biochar in soil environment due to its unknown adsorption capability and content of potentially leachable heavy metals, which are also worth investigation. Based on the literature review, the following research questions are identified:

1. What are the microwave heating characteristics of RDF, the yield and properties of biochar derived from MACP of RDF by adding different types and loadings of catalysts (K_2CO_3, K_3PO_4, bentonite and clinoptilolite)?
2. How do operating conditions affect the yield and pore properties of RDF derived biochar?
3. What is the adsorption performance of biochar derived from MACP of RDF?
4. Does the content of contaminants in RDF derived biochar meet the threshold requirements on soil applications?

Inferred from literature results on other biomass feedstock, the following hypotheses are proposed:

1. Adding those catalysts will significantly improve microwave heating rate and biochar of high specific surface area could be obtained, especially with the addition of K_2CO_3.
2. The pyrolysis temperature will have a great impact on biochar yield and properties, followed by microwave power input and microwave radiation time.
3. The biochar with high specific surface area and large pore volume will have better adsorption capacity, which is especially expected when K_2CO_3 is added.
4. RDF and used catalysts may contain some heavy metals, but biochar may stabilize those heavy metals, preventing them to be released in soil applications.

The main objective of this project is to improve pyrolysis performance of RDF in MACP by applying multi-functional catalysts so as to produce high quality biochar. To achieve the research objective, following research tasks are to be carried out:

1. Characterization of RDF feedstock, including particle size distribution, proximate and ultimate analysis, and thermogravimetric analysis (TGA).
2. Examination of K_2CO_3 and K_3PO_4, as well as their mixtures with bentonite and clinoptilolite, respectively, as catalysts for the MACP of RDF under the same operating conditions to improve pyrolysis performance, biochar yield and biochar quality.
3. Identification of the suitable catalyst or catalyst mixture based on pyrolysis performance, biochar yield and biochar properties.
4. Determination of suitable operating conditions, i.e., microwave power input, targeted pyrolysis temperature and microwave irradiation time, to produce biochar with high specific surface area for the selected catalyst.

5. Comparison with conventional pyrolysis of RDF and MACP of sawdust using the same catalyst under the same operating conditions in terms of heating performance and biochar properties.
6. Adsorption of methylene blue to evaluate the adsorption performance of biochar and batch leaching test to identify the amount of leachable heavy metal contents in biochar.

The thesis is structured that the experimental methods and setup are introduced in Chapter 2, and results and discussions are presented in Chapter 3 and Chapter 4. General conclusions and some future work are summarized in Chapter 5.

Chapter 2: Experimental methods and setup

This chapter describes the preparation of test samples, experimental setup and methodologies to carry out research tasks to achieve proposed objectives. RDF and selected catalysts are well-mixed to make samples for MACP. Various characterization methods have been applied to evaluate RDF and biochar properties, including proximate and ultimate analysis, thermogravimetric analysis (TGA), Brunauer-Emmet-Teller (BET) analysis, Fourier-transform infrared spectroscopy (FTIR), etc. Analysis of Variance (ANOVA) is applied to investigate the statistical significance on the impact of different operating conditions on biochar yield and surface area.

2.1 Sample preparation

The RDF feedstock in this study was obtained from Kawagde Tech Co. LTD in Japan. The raw pellets were a mixture of 30% to 40% wood chips, paper and fiber scraps and 60% to 70% waste plastics. The calorific value of the compacted fuel was in the range of 5,000 kcal/kg to 7,500 kcal/kg. The moisture content was estimated to be 5% or less, whereas the ash, volatile, fixed carbon and C, H, O, N contents of RDF are provided in Table 4.1.

K_2CO_3 (Potassium carbonate, reagent grade ≥98%, -325 mesh), K_3PO_4 (Potassium Phosphate Tribasic, reagent grade ≥98%) and bentonite were purchased from Sigma-Aldrich Canada Ltd. Clinoptilolite was purchased from United States Antimony Corporation. All catalysts are in powder forms and directly mixed with RDF feedstock without any pretreatment.

A large blender was used to crush RDF pellets into small particles which were then dried at 105 °C for 24 h. Afterwards, 10 g RDF particles was well mixed with catalysts at different loadings

(10, 20, 30 wt.%) in a small blender. The prepared mixtures are test samples, which can be poured into a quartz tube reactor using a funnel before the experimental test. Figure 2.1 shows the sample at different stages.

(a) (b) (c)

Figure 2.1 (a) Original, (b) crushed and (c) well-mixed sample.

About 50 g pre-dried RDF particles were screened in an electronic shaker (shakes 30 mins triplicates) to obtain the particle size distribution (PSD), with the data shown in Table 2.1. Most of the RDF particles fell in the range of 0.5 to 2 mm. The PSD of catalysts is shown in Figure 2.2.

Table 2.1 Particle size distribution of ground and pre-dried RDF sample.

Sieve number	Particle size range (mm)	Percent (wt.%)
10	> 2	4.09
14	1.4 – 2	18.42
20	0.85 – 1.4	21.92
35	0.5 – 0.85	18.29
45	0.355 – 0.5	13.33
50	0.3 – 0.355	3.97
60	0.25 – 0.3	3.63
	< 0.25	16.34

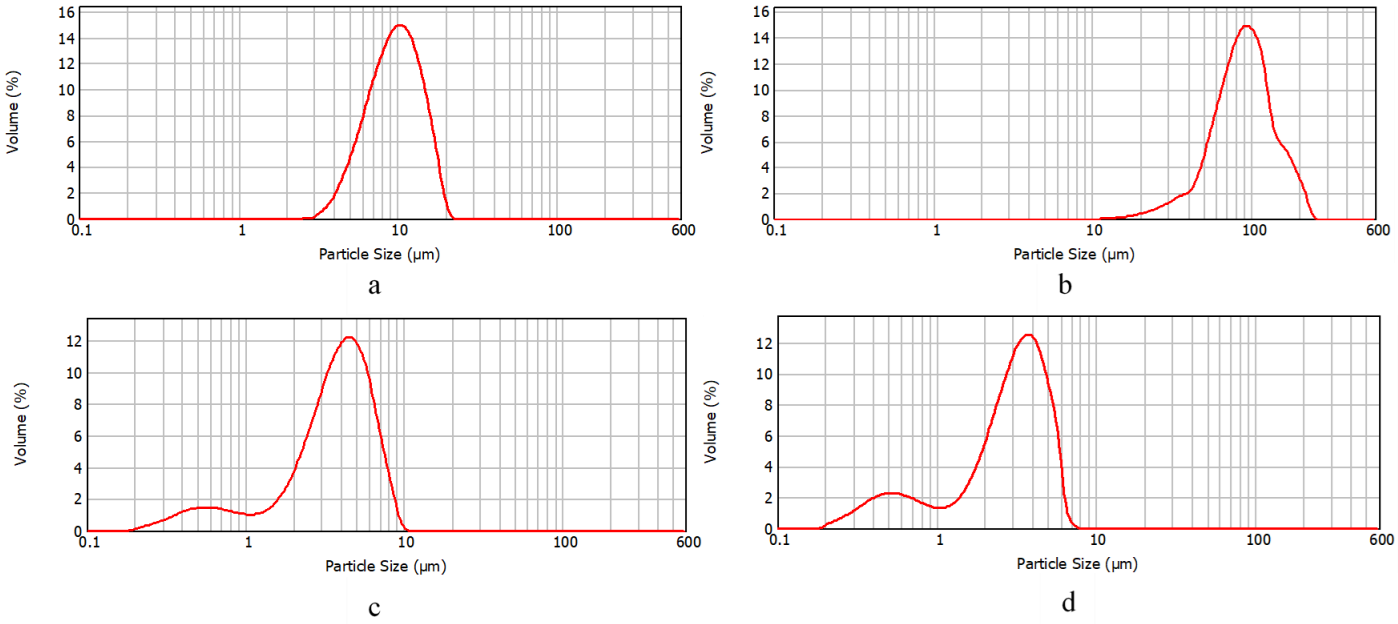

Figure 2.2 Particle size distribution of pre-dried (a) K_2CO_3, (b) K_3PO_4, (c) bentonite, (d) clinoptilolite sample.

2.2 Experimental setup and procedures

Pyrolysis of pure RDF and premixed RDF-catalyst(s) samples were performed in a fixed bed microwave reactor manufactured by Enwave Corporation, Vancouver, Canada. The schematic diagram and a front view of the microwave unit are given in Figures 2.3 and 2.4, respectively. The setup was composed of six sub-systems: microwave generator and reactor system, microwave leakage detection system, vapor condensation and ventilation system, water cooling system, inert gas purging system and PIC control system. A magnetron was installed inside a cabin at the right end of the waveguide to generate microwave. The microwave power input (2.45 GHz, maximum 1200W) could be adjusted by the software installed in a desktop computer linked to the microwave power meter. At the left end of the waveguide, a water jacket (not indicated in the flow chart) was used to absorb the microwave not absorbed by the sample. In case of any microwave leakage exceeding the safety limit, a microwave detector connected to an auto-locked microwave leakage monitor would cut off the power. The reactor chamber was insulated to reduce heat loss. A

cylindrical quartz tube (44 mm ID × 48 mm OD × 245 mm height) was used as the reactor installed vertically inside the reactor chamber, with both ends of the tube tightly connected to the inlet and outlet tubes with O-ring and stainless steel sealers. As microwave interacts with metallic walls of thermocouples, an infrared pyrometer was placed on the top of the reactor to measure the sample temperature in the quartz tube with the signal acquired by PIC data acquisition system. A camera was also installed above the reactor to monitor the upper surface of the sample in the quartz tube reactor during pyrolysis. Nitrogen from the gas cylinder (grade 5.0, ≥99.99%) supplied from Praxair Canada Incorporation was used to maintain inert atmosphere inside the reactor system and to prevent fouling of the infrared pyrometer. There are four water loops with a main control valve and adjustable rotameter on a side panel for cooling the infrared pyrometer, magnetron and pyrolysis vapors by two condensing tubes. Bio-oil is condensed and the non-condensables are directly vented to a fumehood.

For each test, after the sample is securely loaded inside the reactor, N_2 gas valve was adjusted to 1.5 L/min for 30 min to purge the air out of the reactor system. The water cooling system was also turned on at 2 L/min flow rate for 2 mins to ensure it is working properly. During the purging

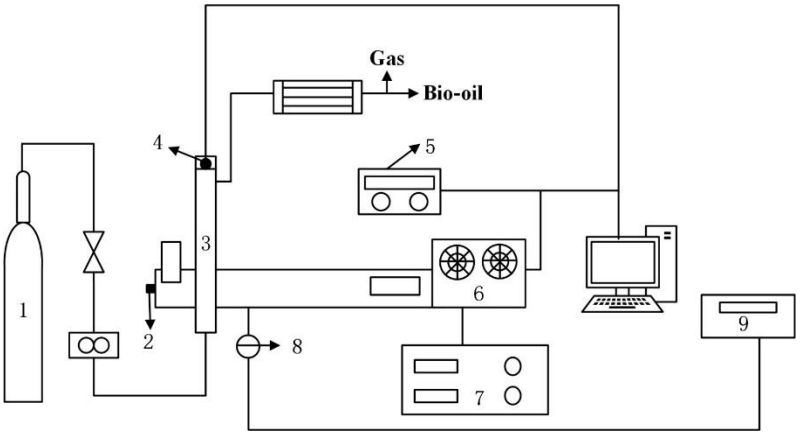

1. Nitrogen cylinder
2. Camera
3. Reactor body
4. Infrared pyrometer
5. Microwave power meter
6. Magnetron
7. PIC control
8. Microwave leakage detector
9. Microwave leakage monitor

Figure 2.3 Schematic diagram of the microwave unit.

Figure 2.4 Front view of the microwave unit.

period, the heating tape wrapped the outlet tube was pre-heated to 350 °C, aiming to prevent vapor condensation that may foul and block the tube. When purging was finished, the PIC control panel, microwave power meter, water cooling system and data acquisition program were all started, and the N_2 gas line for protecting the infrared pyrometer was adjusted to 0.5 L/min. Specific microwave power was then applied to heat the sample to targeted pyrolysis temperature, after which microwave power was reduced to maintain the temperature at the target level until completion of pyrolysis. After the microwave power is shut down at the end of the test run, the cooling water and N_2 gas continued running until the inner temperature of the reactor is cooled down to room temperature. The solid residues, biochar, was discharged from the quartz tube, then soaked in distilled water and filtered to separate the solids and liquid solution. The collected solid sample was dried, weighed and stored in a desiccator. For each case in the experimental design, the average of triplicate tests was reported.

2.3 Experimental design

As shown in Table 2.2, the effects of four parameters on pyrolysis performance are investigated, namely catalysts, microwave power input, targeted pyrolysis temperature and microwave radiation time. Catalyst is the most important parameter that influences the heating performance and biochar properties. Two catalysts (K_3PO_4 and K_2CO_3) and their mixtures with other two catalysts (Bentonite and Clinoptilolite) were mixed with RDF at different loadings to investigate the catalytic effect, under 1200 W microwave power, 550 ℃ pyrolysis temperature and 30 mins microwave radiation time. Based on biochar properties (especially specific surface area), heating performance and biochar yield among these cases, the optimal catalyst is determined and then further evaluated against other operating parameters. The heating rate is controlled by the microwave power input and is investigated prior to investigating the temperature and time effects. At the optimum microwave power input, the effects of pyrolysis temperature and microwave radiation time on biochar yield and properties are investigated.

Table 2.2 Experimental parameters investigated in MACP of RDF.

Catalyst(s) (mixing ratio: wt.%)		Microwave power (W)	Pyrolysis temperature (℃)	Microwave radiation time (min)
K_3PO_4	K_2CO_3			
0	0	1200	550	30
10	10	1100	500	60
20	20	1000	450	120
30	30	900	400	
20+10bentonite	20+10bentonite	800		
20+10clinoptilolite	20+10clinoptilolite	700		
0+30bentonite	0+30clinoptilolite	600		

To compare the heating performance, biochar yield and biochar properties of RDF and sawdust, MACP of RDF and sawdust are performed under the same conditions, i.e. same amount of feedstock, same catalyst and same operating conditions. To compare the yield and properties of biochar produced from conventional pyrolysis and MACP, conventional pyrolysis of RDF in an electrically heated furnace is carried out under the same pyrolysis conditions as MACP.

2.4 Characterization

2.4.1 Thermogravimetric analysis

Thermogravimetric analysis (TGA) of crushed and pre-dried RDF samples was conducted using a Shimadzu TGA-50 thermogravimetric analyzer (Mandel Scientific, Canada) in an inert atmosphere, with 50 ml/min N_2 flow rate. In each test, ~10 mg sample was loaded into an alumina ceramic crucible and heated up at the rate of 10 °C/min from room temperature to 600 °C, then maintained for 30 min. The weight was recorded every 1 s and the accuracy of the balance was 0.01 mg. Tests were done triplicates to ensure reproducibility of TGA results.

2.4.2 Proximate and elemental analysis

The proximate and ultimate analyses of pre-dried RDF, sawdust and biochar sample were implemented to determine the sample composition. The volatile and ash content were measured according to ASTM D7582. About 0.5 g of the sample was weighed and loaded into a crucible, then heated in N_2 atmosphere at 925 °C for 7 min in a muffle oven. The percentage of weight loss was recorded as the volatile matter content. Another 0.5 g of the sample was heated in air at 575 °C for 2 h and the fraction of the remaining solid was recorded as ash content of the original sample. Carbon, hydrogen and nitrogen contents were determined by Thermo Flash 2000

Elemental Analyzer and reported on dry-ash free basis. The fixed carbon and oxygen content were calculated by difference.

The elemental composition of the original biochar sample was measured using an ICP-7510. The weighed sample (0.1 g) was digested with 10 ml aqua regia, 5 ml HF and $HClO_4$ and the solution was heated on an electric furnace to be concentrated to around 1 ml. Finally, the leftover solution was diluted in a volumetric flask (50 ml) and analyzed by Inductively coupled plasma atomic emission spectroscopy (ICP-AES).

2.4.3 Pore properties and morphology

The specific surface area of biochar was measured by N_2 adsorption/desorption isotherm at 77 K on a Micromeritics ASAP 2020 instrument. First, 0.4~0.5 g biochar sample was degassed under vacuum atmosphere at 150 °C for 8 h on the built-in degassing port of the instrument. After degassing, the sample was weighed again and recorded as the real mass before analysis. The total surface area and average pore diameter were determined by Brunauer-Emmet-Teller (BET) analysis, whereas the micropore area and volume were determined by Barette-Jovner-Halenda (BJH) method. The morphology of biochar samples was examined by scanning electron microscopy (SEM) on a Philips XL30 electron microscope.

2.4.4 Functional groups

The functional groups of biochar were measured by Fourier-Transform Infrared Spectroscopy (FTIR). Approximate 0.1 g of the sample was ground to fine powders and pressed

into slices. The prepared slices were measured on a Bruker Vertex 70 Spectrometer in the range of 400-4000 cm^{-1} at a resolution of 4 cm^{-1} with 64 scans in total.

2.4.5 Methylene blue adsorption

Methylene blue (MB) was selected as the representative model adsorbates to identify the adsorption abilities of biochar. For each test, 0.01 g biochar sample was well mixed with MB solution (concentration: 7.5*E-5 M, volume: 20 ml) in a conical flask and then agitated for 1 h on an electrical stirrer. After shaking, the solution of liquid and solid mixtures was centrifuged at 600 revolutions per minute (rpm) for 20 mins, and then filtered across a membrane filter of 0.2 micron. The filtrate was analyzed using spectrophotometer at maximum 664 nm wavelength of absorbance. The MB removal efficiency was calculated by:

$$E_{MB} = \frac{[A]_I - [A]_E}{[A]_I} \times 100\% \quad (2.1)$$

In which E_{MB} refers to the MB removal efficiency (%), $[A]_I$ and $[A]_E$ are initial and equilibrium MB concentration (M).

2.5 Batch leaching test

The two-stage batch leaching test of biochar samples was carried out according to LST EN 12457-3 standard. The first stage involves soaking and agitating 3 g sample with 100 ml deionized water for 6 h with 200 rpm in a conical flask and then filtering to obtain the leachates. In the second stage, the leachates along with the used filters were put into another flask and agitated for 18 h After each agitation, the flask was left to sit for 40 min for suspended solids to settle before the solution was filtered by a syringe filter of 0.45 micron. The leachates were analyzed by ICP-AES

to determine heavy metal content. The heavy metal content in pure RDF and RDF burned ash samples was also measured and compare with biochar samples.

2.6 Statistical analysis

One-way and two-way analyses of variance (ANOVA) and Tukey's honestly significant difference (HSD) post hoc tests were employed to identify the statistical significance of the impact of operating conditions on biochar yield and specific surface area, as well as the interactions between targeted pyrolysis temperature and heating time. The descriptive table was generated with 95% confidence level and the ANOVA table was used as the criteria to determine possible statistical significance between parameters at 95% confidence level ($p < 0.05$). According to calculated F values, the dominant parameter influencing the biochar specific surface area could be determined. All statistical analysis was implemented on IBM SPSS Statistics software.

Chapter 3: Microwave-assisted catalytic pyrolysis of RDF

This chapter mainly investigates the heating performance of RDF using different catalysts and microwave power under typical pyrolysis conditions. Based on the decomposition behavior of RDF at different temperature range by TG shown in Figure 3.1, 550 °C is chosen as the final controlled temperature in all the following tests. The characteristics of microwave assisted catalytic pyrolysis (MACP) is evaluated at different heating stages with a focus on the hotspot phenomenon. Heating performance of RDF and its mixture with K_2CO_3 or K_3PO_4 at different ratios is first analyzed, followed by the performance with the addition of bentonite or clinoptilolite as the secondary catalyst. Furthermore, microwave power is varied to examine its effect on hotspot phenomenon and reaction rate using RDF mixed with 20 wt.% K_2CO_3 and 10 wt.% bentonite.

3.1 Pyrolytic properties of RDF

TGA of pure RDF was performed to identify its pyrolytic behavior so as to select the operating conditions of MACP of RDF. As shown in Figure 3.1, there were no significant changes in weight loss before 200 °C because the sample was pre-dried. RDF began to decompose at about 200 °C. The weight loss rate from DTG curves started to increase with some fluctuation until 350 °C. Over this period, cellulose, hemicellulose and lignin, the key components in wood and paper contained in RDF, start to break down to light volatiles (Cozzani et al., 1995a). The first peak at 350 °C could be attributed to the decomposition of majority of cellulosic components, whereas the second peak at ~410 ^{o}C was mainly due to the devolatilization of plastics. The sample weight remained nearly constant beyond ~500 °C, suggesting that most of the pyrolysis reactions completed at around 500 °C. This temperature range corresponds to the depolymerization of plastics, which largely consists

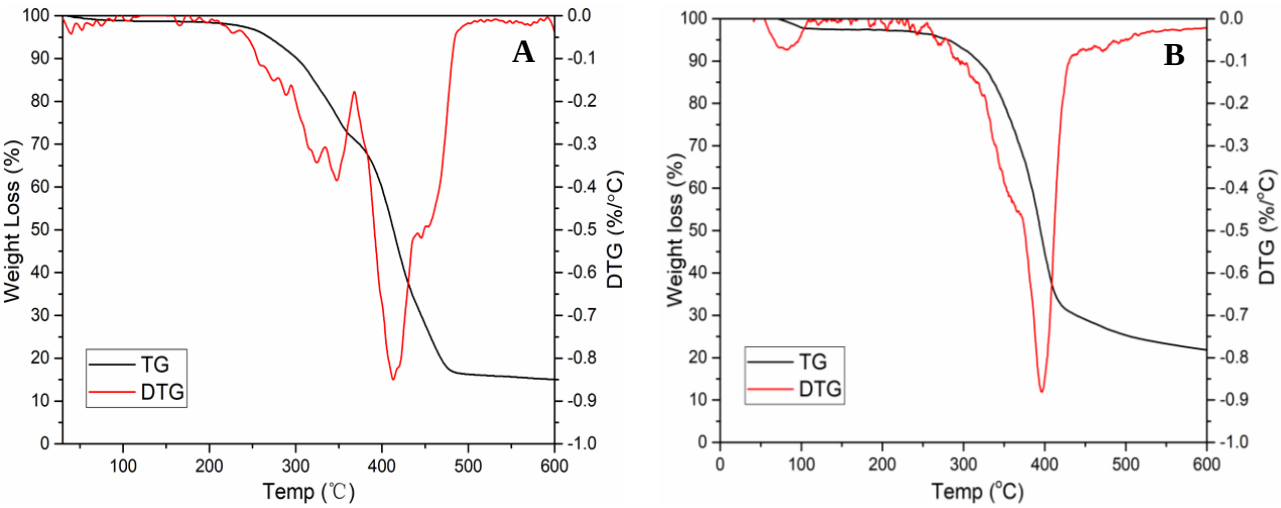

Figure 3.1 TG and DTG results of pre-dried RDF sample (A) and original sawdust (B).

of RDF (Cozzani et al., 1995b). Compared with TGA of woody biomass, sawdust exhibited a relatively single peak around 400 °C in the range of 200 °C to 600 °C. The weight loss rate was much lower than that of RDF between 400 °C and 500 °C. The decomposition temperature of different components in RDF can be found in Table 3.1 (Bach et al., 2015; Bach and Chen, 2017; Singh et al., 2012; Yang et al., 2007). It is desirable to destruct these plastics components to obtain high quality biochar, because those polymers remaining in the product may block pore structures of biochar. It has been reported that a low temperature caused inadequate pyrolysis and failed to create various micro-channels in biochar (Cheng and Li, 2018). Therefore, the suitable temperature for pyrolysis of RDF is set to be 550 °C in this study to allow for complete conversion of RDF.

Table 3.1 Decomposition temperature of different components in RDF.

Components	Decomposition temperature range	Decomposition temperature peak
Hemicellulose	200-360 °C	~300 °C
Cellulose	250-400 °C	~350 °C
Lignin	200-600 °C	~400 °C
Waste plastic	400-500 °C	~470 °C

The weight loss characteristics of RDF in this study is generally in accordance with previous TGA work on RDF except the second decomposition temperature peak for plastics that was found around 470 °C in other studies (Seo et al., 2010; Singh et al., 2012), which was probably due to the heterogeneous compositions of plastics in RDF from different sources. The decomposition temperature peak of 470 °C was reported to correspond to pure PVC (470 °C), LDPE (472 °C) and HDPE (479 °C) (Grammelis et al., 2009), while 410 °C was close to the decomposition temperature of pure PS and PET (Singh et al., 2019). Therefore, it is suspected that PS and PET may be the main components of waste plastics in RDF used in this study. TGA results also provided some useful information on volatiles content in RDF sample, which is approximately 84%. This implies that the yield of solid residues after pyrolysis may be very low. However, the biochar yield may also be influenced by operating conditions (e.g. microwave power intensity, targeted pyrolysis temperature and microwave radiation time), which needs to be investigated.

3.2 Pyrolysis behavior of RDF in MACP

In conventional pyrolysis, the feedstock is normally heated up from ambient temperature to a high temperature at a constant heating rate and is then maintained at that level for some time to promote further reaction. However, as shown in Figure 3.2, the heating rate was not constant at a constant microwave power in MACP, including three stages: slow pre-heating, rapid heating and constant temperature stage. The first two heating stages are divided by the hotspot phenomenon, whereas the third stage corresponds to the approach to the set constant temperature.

In the pre-heating stage for biomass feedstock mixed with small amounts of catalyst that have better dielectric properties, catalyst can absorb more microwave irradiation, generate and transfer

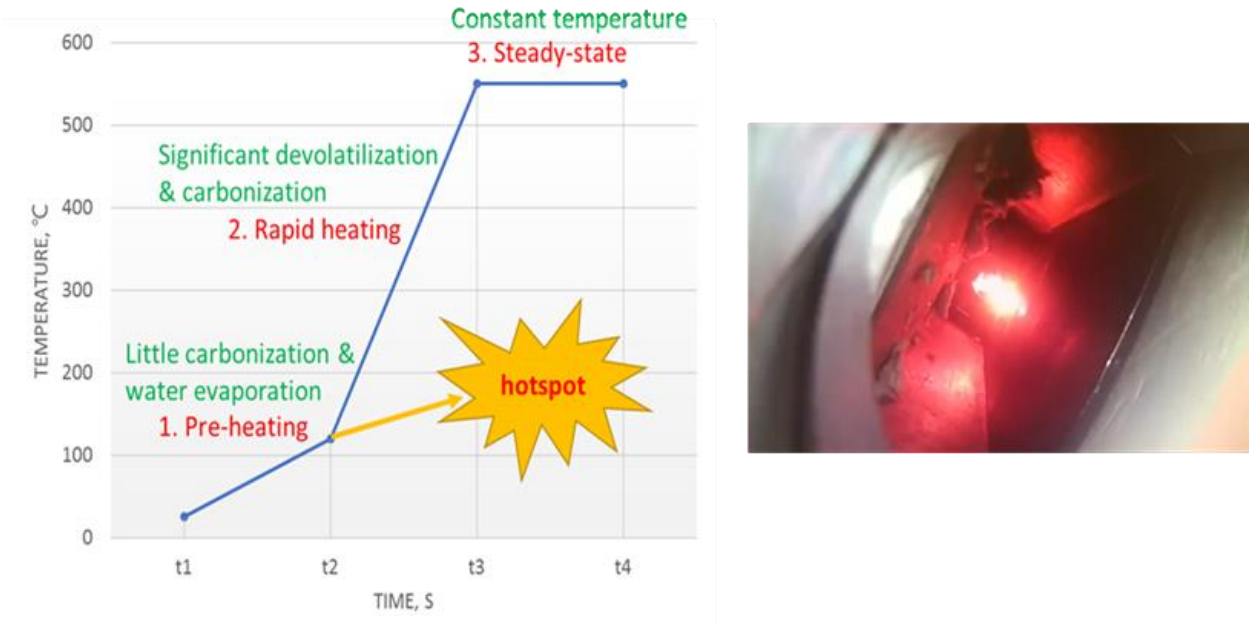

Figure 3.2 MACP stages and hotspot phenomenon.

more heat to surrounding biomass through conduction and convection. As a result, the temperature rises moderately (~60 °C/min) with some smoke generated. Water in biomass also serves as a good microwave absorber which plays an important role in early stage (Mohamed et al., 2016b). The reactions occurring at this stage are mostly dehydration.

Since the catalyst is well mixed with feedstock, catalyst particles inside the feedstock can be assumed to be adequately and evenly dispersed. If the microwave heating is assumed to be uniformly distributed to the samples, heat generation can be considered as uniform as well. However, for a packed bed of particles, heat needs to be transferred out toward the cold wall, creating a potential high temperature zone in the middle of the packed particles. As a result, a region of very high temperature can form which is called the "hotspot" in this study. Besides, the non-uniform distribution of microwave electromagnetic field may also promote the hotspot formation (Huang et al., 2016). In a small-scale unit, hotspot can trigger the pyrolysis/oxidation

reaction, initiating a jump in temperature over a relatively short period (Jones et al., 2002). Thus, the presence of hotspot is essential in lab scale experiments to initiate pyrolysis. Otherwise the pyrolysis reaction may not be started.

The hotspot phenomenon represents the beginning of pyrolysis which involves a series of irreversible thermo-cracking reactions, as mentioned in TGA results (Section 3.1). In MACP of RDF, large amount of white smoke is generated at stage 2 from the reactor after the pyrolysis reaction is initiated and most of the biochar is produced in this stage. Catalysts are believed to have a dominant effect not only on the heating rate but also on the cracking and carbonization. However, due to the dehydrogenation of alkanes and condensation of aromatic species which occur at the same time with cracking reactions, catalysts may be deactivated quickly because of the formation of coke on their surface, leading to an incomplete conversion to biochar (Kucora et al., 2017). The heating demand will decrease when the temperature approaches the set targeted temperature.

It is also observed that during pre-heating and rapid heating periods temperature may not always increase. The temperature fluctuations can be caused by the changing of dielectric properties of biomass/biochar and the coke formation on the catalyst surface as well as some endothermic reactions during the rapid heating process (Mohamed et al., 2016b), which will be discussed in the MACP of RDF results section.

When temperature approaches the targeted value, microwave power input can be adjusted and controlled to maintain a constant temperature with variations less than ±5°C. The time duration over constant temperature period is defined as the pyrolysis residence time in this study and it is

mainly dependent on the hotspot onset time and average heating rate in rapid heating stage if the total microwave radiation time and targeted pyrolysis temperature are specified.

3.3 Effect of catalysts on heating performance of RDF

Due to different dielectric properties and catalytic effect of catalysts, the heating performance of RDF mixed with different catalysts varied in terms of hotspot onset time, average heating rate, maximum final temperature etc. Besides, mixing K_2CO_3 or K_3PO_4 with bentonite or clinoptilolite may demonstrate synergistic effects on improving microwave heating rate based on previous study of Mohamed et al. (2016).

3.3.1 Single catalyst

The heating performance of pure RDF and RDF mixed with 10, 20, 30 wt.% of K_2CO_3 and K_3PO_4 is shown in Figure 3.3. At a first glance, all curves in Figures 3.3 (a) and (b) seem to follow a general trend. During the pre-heating stage, temperature rose up first because of the absorption of microwaves by water and catalyst, then decreased slightly for some time before hotspot appeared. At this point, a cloud of white smoke was generated as observed in the downstream vapor condensing tube and flasks. A possible explanation is that as the microwave radiation absorbed by the sample (mainly catalyst), heat is generated and transferred to surrounding RDF particles through conduction primarily, leading to the temperature rise. When the temperature reaches 100-120 °C, relatively unstable compounds start to decompose with light gas molecules such as H_2O, H_2, CO and CH_4 released from the sample. Some of those reactions may be endothermic, which consume microwave energy and change the heat balance. Meanwhile, the released gas cloud may also interfere the temperature measurement of the infrared pyrometer because the absorption of IR

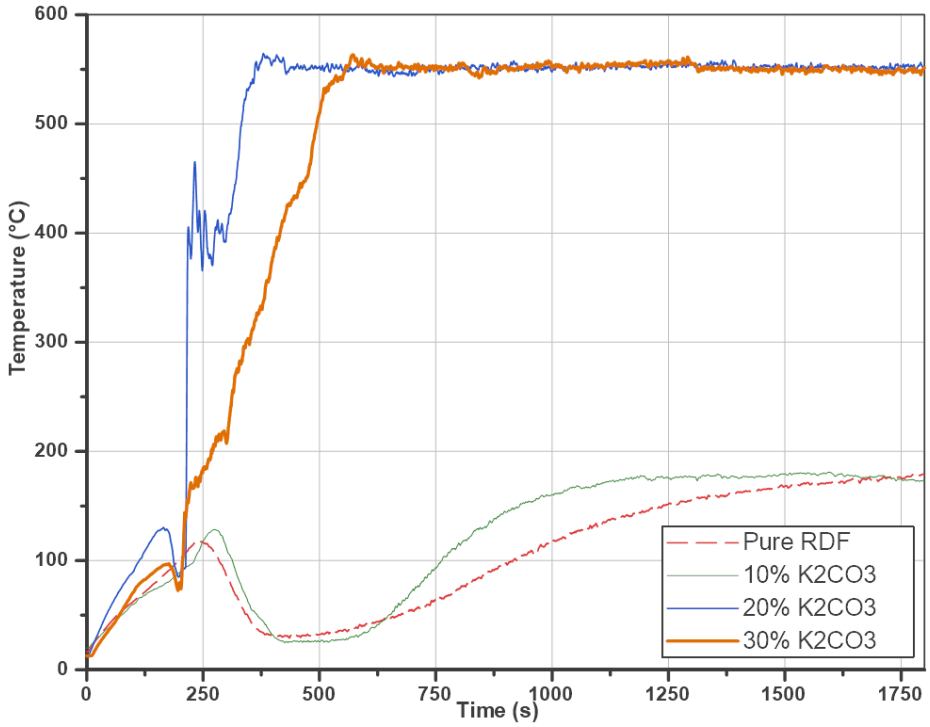

(a)

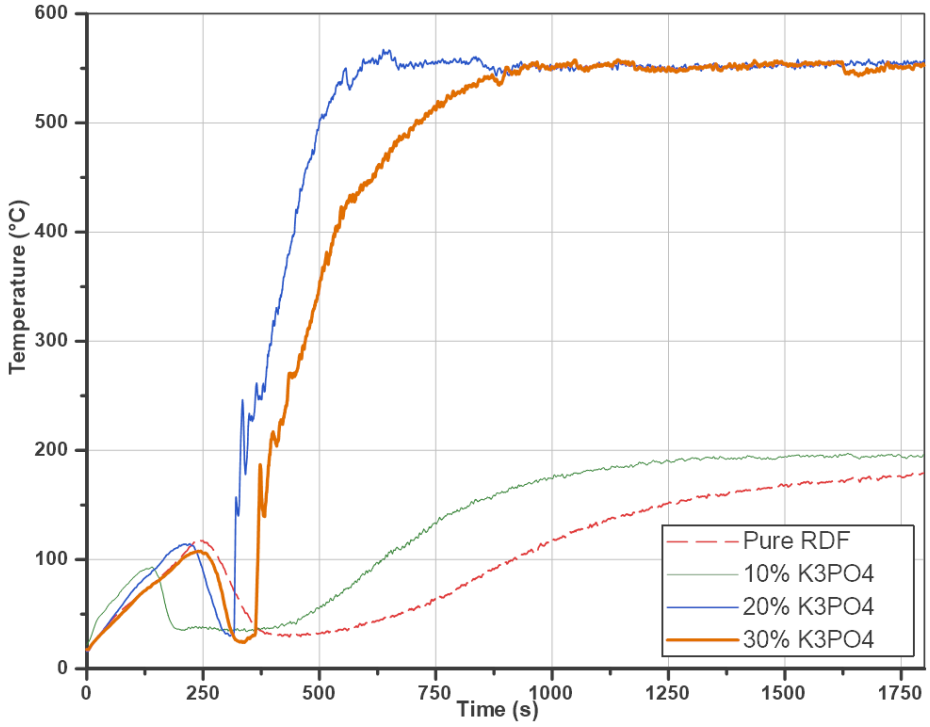

(b)

Figure 3.3 Heating performance of pure RDF and RDF mixed with 10, 20 and 30 wt.% of (a) K_2CO_3 and (b) K_3PO_4 (microwave power: 1200 W).

waves by some greenhouse gases in the gas cloud, such as H_2O, CH_4, CO and CO_2, may block or reduce the IR light to reach the sample surface for proper temperature measurement of the pyrometer. Owing to the poor microwave absorption of pure RDF, no hotspot was generated at the end of the pre-heating stage. The temperature slowly went up and reached a final temperature of 180 °C only, failed to initiate pyrolysis. Similar results were found for samples with 10 wt.% K_2CO_3 and 10 wt.% K_3PO_4, because of too low catalyst amount to absorb enough microwave. Another possible cause is related to the large separation distance among bulky RDF particles which are quite fluffy after crushed. This leads to very poor heat transfer among RDF particles and catalyst particles.

For RDF samples containing 20 wt.% and 30 wt.% K_2CO_3, hotspot appeared around almost the same time (3.8 min) and temperature rose sharply afterward, especially for 20 wt.% K_2CO_3 which reached a transient heating rate of 45 °C/s. Clearly, 20 wt.% K_2CO_3 had a higher average heating rate (184 °C/min) and reached the final temperature of 550 °C earlier (at 6 min) than 30 wt.% K_2CO_3 over the rapid heating stage, although some severe fluctuations occurred around 400 °C. These fluctuations can be attributed to the endothermic decomposition reactions of cellulosic materials and plastics during this rapid heating stage. K_3PO_4 shared similar trends with K_2CO_3, but the hotspot appeared later and the sample took longer time to reach 550 °C. There were less severe fluctuations for the 30 wt.% K_2CO_3 and K_3PO_4 samples than the 20 wt.% K_2CO_3 sample in the rapid heating stage, possibly due to a relatively higher heat generation rate in a slower heating process.

In general, for the cases where pyrolysis was initiated successfully, two conclusions can be drawn from Figure 3.3: (1) K_2CO_3 showed better heating performance than K_3PO_4; (2) 20 wt.% potassium catalyst gave better heating performance than 30 wt.%. K_2CO_3 has better dielectric properties than K_3PO_4 and has been often used for microwave activation of biochar to produce activated carbon (Foo and Hameed, 2012c; Tay et al., 2009). The proposed chemical reactions for K_2CO_3 in an inert atmosphere are as follows (McKee, 1983):

$$K_2CO_3 + 2C \rightarrow 2K + 3CO \quad (3.1)$$

$$K_2CO_3 \rightarrow K_2O + CO_2 \quad (3.2)$$

$$K_2O + 2C \rightarrow 2K + CO \quad (3.3)$$

Those reactions provide a clear insight on the functionality of K_2CO_3 during pyrolysis not as a catalyst but as an activating agent. The formation of potassium compound would diffuse into the solid char structure and widen the pores, whereas produced gases break through the walls and create new channels in biochar microstructure, leading to a high surface area and pore volume. However, excess K_2CO_3 is not encouraged because it reacts with carbon which results in a lower biochar yield (Foo and Hameed, 2012a). On the other hand, PO_4^{3-} is more stable and less reactive than CO_3^{2-}. Thus, K_2CO_3 is better than K_3PO_4 in terms of accelerating microwave heating and producing biochar of higher surface area and more porous structure.

It has been reported that 20 wt.% alkali metal salts generate coke and gas production, and potassium catalyst benefits Equations (3.4) and (3.5) (Zhao et al., 2014). Those endothermic reactions will decrease the heating rate during rapid heating stage. Meanwhile, the deposited coke on catalyst surface may abate its microwave absorption capacity, reducing the conversion of microwave irradiation into heat. The same phenomenon was also observed and discussed in

Mohamed et al. (2016b). In addition, PO_4^{3-} undergoes transformation to P_2O_5 but requires high activation energy, leading to extended pyrolysis time (Villota et al., 2018). Therefore, 20 wt.% potassium salt appears to be a good catalyst load and is selected as the basis for tests mixed with bentonite and clinoptilolite.

$$C(s) + CO_2(g) \rightarrow 2CO(g),\ \Delta H_{298K} = 173\ kJ/mol \quad (3.4)$$

$$CH_4(g) + CO_2(g) \rightarrow 2CO(g) + 2H_2(g),\ \Delta H_{298K} = 260.5\ kJ/mol \quad (3.5)$$

3.3.2 Catalyst mixtures

Figure 3.4 compares the heating performance of RDF mixed with 20 wt.% K_2CO_3 or K_3PO_4 and 10 wt.% bentonite or clinoptilolite. After adding bentonite or clinoptilolite into potassium salts, no significant changes were observed among those tested cases. The hotspot of 20 wt.% K_2CO_3 + 10 wt.% clinoptilolite appeared earlier by ~4 min than other cases. At the rapid heating stage, compared with 20 wt.% single potassium salts (Figure 3.3), the addition of 10 wt.% bentonite or clinoptilolite shifted the temperature fluctuations to higher temperatures (from ~400 °C to 450 °C for K_2CO_3 and from ~200 °C to 300 °C for K_3PO_4) and lowered the amplitude of fluctuations. Bentonite and clinoptilolite may play an important role in generating and transferring heat more effectively to create a more uniform temperature throughout the reaction system (Sulman et al., 2009). It may also delay some catalytic endothermic reactions to higher temperatures. Reactor temperature in all cases reached 550 °C at about 8 minutes. In this work, the average heating rates from hotspot initiation point to the targeted temperature over the rapid heating stage were calculated from the average of instantaneous heating rate (v=dT/dt) with results given in Table 3.2. Heating rate of RDF mixed with 20 wt.% K_2CO_3 remained the highest (184 °C/min), followed by catalyst mixtures. Clearly, adding bentonite and clinoptilolite slightly decreased the average

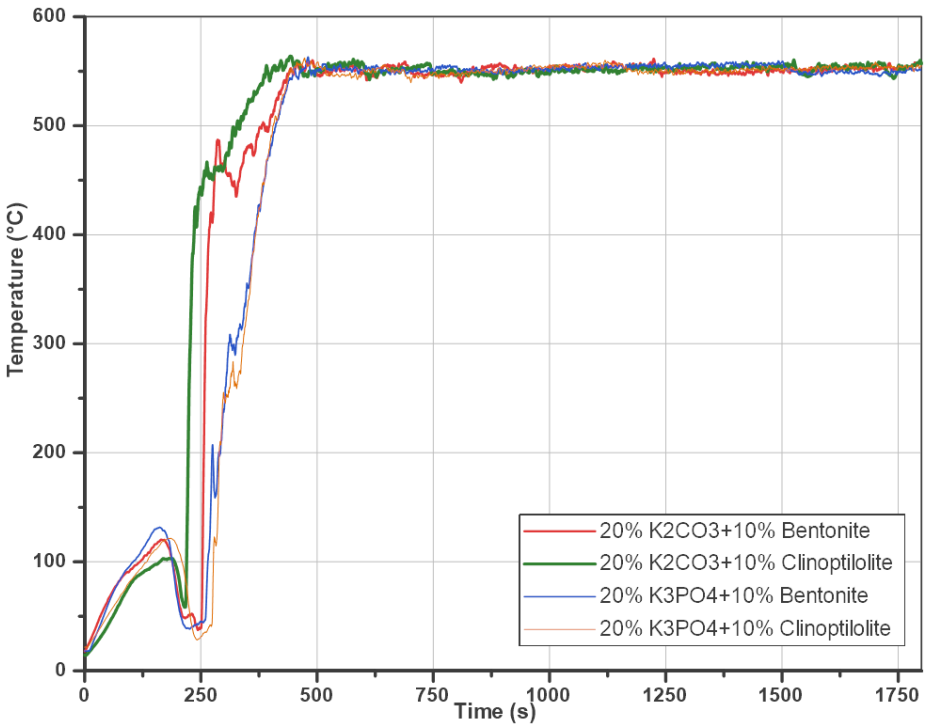

Figure 3.4 Heating performance of RDF mixed with combinations of catalysts (microwave power: 1200 W).

heating rate of K_2CO_3 but considerably increased that of K_3PO_4, which proved the synergistic effect on improving heating rate. As K_2CO_3 performed much better than K_3PO_4 in accelerating microwave heating, adding a secondary catalysts into K_2CO_3 could not substantially change the heating performance of RDF.

Table 3.2 Average heating rate of pure RDF and RDF mixed with different catalysts.

Catalyst (%: wt.%)	Heating rate (°C/min)	Catalyst (%: wt.%)	Heating rate (°C/min)
20% K_2CO_3	184 (±14)	20% K_2CO_3+10% bentonite	163 (±20)
30% K_2CO_3	82 (±21)	20% K_2CO_3+10% clinoptilolite	173 (±22)
20% K_3PO_4	115 (±16)	20% K_3PO_4+10% bentonite	167 (±17)
30% K_3PO_4	57 (±9)	20% K_3PO_4+10% clinoptilolite	181 (±14)
10% K_2CO_3	13 (±3)	0% (pure RDF)	6 (±2)
10% K_3PO_4	11 (±4)		

In MACP, due to the very poor dielectric properties and heat transfer of RDF, sample heating rate is mainly dependent on the added catalyst(s). The catalyst absorbs most of the microwave irradiation and converts it into heat, then transfers heat to surrounding particles through conduction, which results in the temperature rise. Therefore, the effect of catalyst on heating rate can be divided into two main aspects: microwave absorption (dielectric constant, ε) and heat conversion or dissipation (dielectric loss) capabilities and thermal conductivity of catalyst. Bentonite is one of smectite class natural clays with a composition of silica, alumina, iron, calcium and potassium. Clinoptilolite is a natural zeolite comprising of a microporous arrangement of silica and alumina tetrahedra. Compared with K_2CO_3 and K_3PO_4, the ionic compounds with higher dielectric constant and better microwave absorption capability, bentonite or clinoptilolite does not have good microwave absorption capacity. However, they are notable heat transfer media, which can assist in improving heat transfer rate from K_3PO_4 to RDF (Mohamed et al., 2019). This was proved in the preliminary tests on MACP of RDF where for RDF mixed with 30 wt.% bentonite or clinoptilolite, no hotspots were identified and the maximum final temperature was lower than 200 °C (see Appendix A).

In fast pyrolysis, a high heating rate is required to increase liquid yield and suppress slow side reactions (Schwenke et al., 2015). On the other hand, biochar yield would decrease with increasing heating rate, because of the thermal decomposition of large molecular weight hydrocarbons contained in solid residue (Efika et al., 2015). In catalytic pyrolysis, the heating rate may not have a direct and clear relationship with biochar properties because of the catalytic effect, which will be discussed in section 4.1. Last but not least, although bentonite and clinoptilolite offer similar functions on promoting heat transfer, they impact largely on pore properties of produced biochar.

3.4 Effect of microwave power intensity

Figure 3.5 shows the influence of microwave power intensity on the heating performance of RDF mixed with 20 wt.% K_2CO_3+10 wt.% bentonite. There was no hotspot, and the maximum temperature was recorded as 206 °C at 600 W microwave power, as a result of insufficient microwave energy input. Hotspot was identified in all other cases at different time, ~8 minutes for 700 W and ~4 minutes for 1000-1200 W. With 700 W microwave power, the average heating rate was quite low and it took a long time to reach required final temperature, mainly because of the heat consumed by endothermic decomposition reactions at the temperature range from 350 °C to 500 °C. The temperature reached 550 °C at ~10 min for 800 W and 1000 W microwave power, whereas it took only ~7 min to reach the target temperature for 1100 W and 1200 W microwave power. The average heating rate was calculated for those cases and reported in Table 3.3. Clearly,

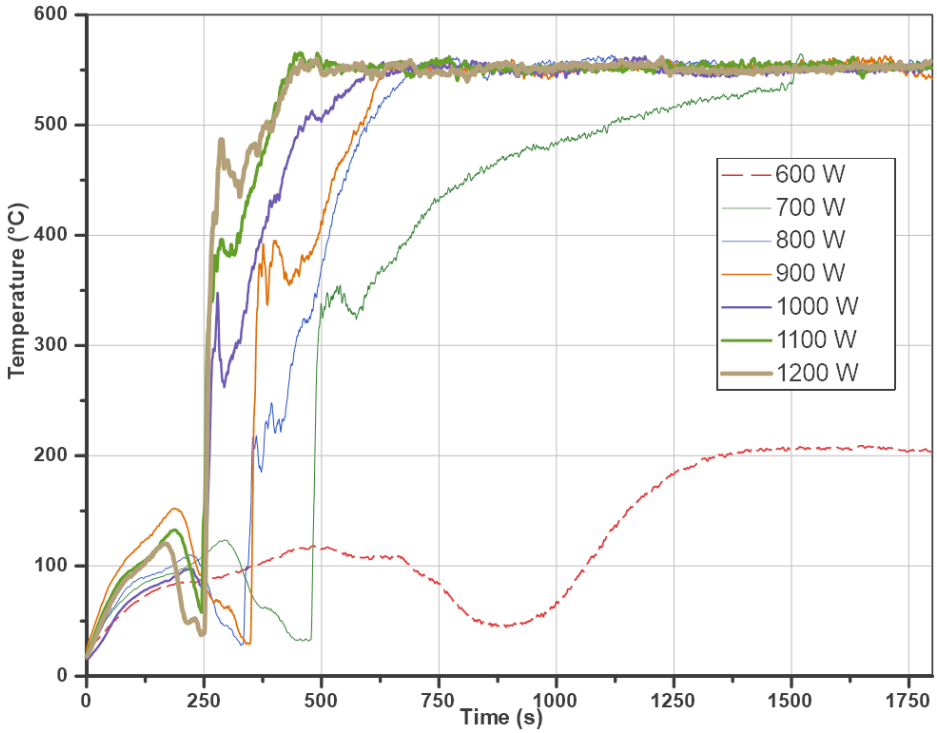

Figure 3.5 Heating rates of RDF mixed with 20% K_2CO_3 + 10% bentonite under different microwave power intensity.

the heating rate is positively correlated with microwave power, but not linearly, which may be due to the non-linear relationship between microwave absorption and the microwave irradiation intensity or the non-uniform distribution of the RDF and catalyst sample.

As the average heating rate in rapid heating stage is dependent on microwave power intensity using the same catalyst under the same operating condition, the impact of heating rate on the yield and pore properties of biochar can be evaluated using biochars produced at different microwave power intensity (from 700 W to 1200 W) in MACP of RDF, which will be presented in Chapter 4.

Table 3.3 Average heating rate of RDF mixed with 20% K_2CO_3 + 10% bentonite under different microwave power intensity.

Microwave power (W)	1200	1100	1000	900	800	700	600
Heating rate (°C/min)	163 (±20)	150 (±19)	118 (±15)	109 (±23)	87 (±18)	30 (±6)	10 (±4)

3.5 Comparisons between RDF and sawdust

As introduced before, RDF sample has low density, heterogeneous composition, poor microwave absorption ability and poor heat transfer, making it quite difficult to be dealt with in thermo-cracking. Its pyrolysis performance is directly compared to sawdust, a widely used biomass feedstock, in Figure 3.6 using the same catalyst and microwave power intensity in MACP. In both the pre-heating and rapid heating stages, sawdust showed a much better heating performance than RDF. Because of its higher bulk density, sawdust particles are more closely packed, making heat transferred more easily, compared to RDF. This explains why high catalysts loading was needed

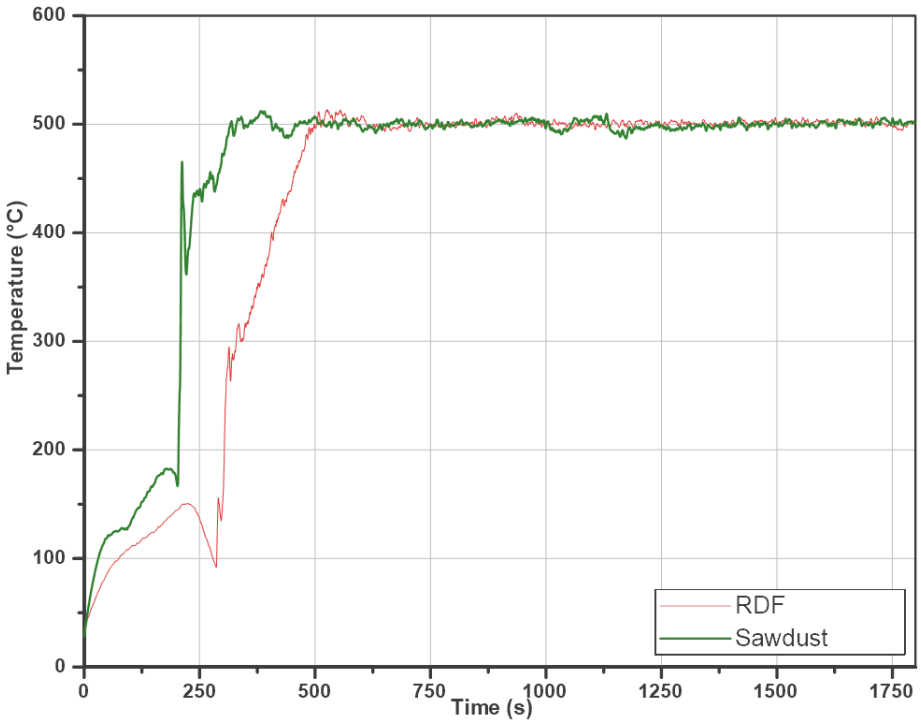

Figure 3.6 Heating rates of RDF and sawdust mixed with 20% K_2CO_3 + 10% bentonite (microwave power: 1000 W).

in heating up RDF in this study, compared to the previous study using biomass samples in the same test unit (Mohamed et al., 2016b). The results also demonstrated the importance in selecting proper catalyst(s) loading and using sufficient microwave power in MACP of RDF.

3.6 Summary

In this chapter, microwave assisted pyrolysis of RDF mixed with different catalyst and catalyst mixtures has been investigated based on the sample heating rate. It is observed that due to the heterogeneity of RDF, decomposition of different components may take place at different temperature ranges, causing fluctuations in weight loss rate and temperature. The successful initiation of pyrolysis was found to correspond to the occurrence of the hotspot. In MACP of RDF, K_2CO_3 showed higher heating rate than K_3PO_4 because of better dielectric properties and catalytic

effect, and 20 wt.% catalyst loading showed better heating performance than 30 wt.%. The heating performance was further improved when a second catalyst, bentonite or clinoptilolite, was added to the RDF sample. Due to poor contact of bulky RDF particles, RDF heating performance was found to be much poorer than sawdust.

Chapter 4: Characterization of biochar

In this chapter, the yield and properties, especially pore properties of biochar produced from MACP of RDF using different catalysts and under various operating conditions are evaluated. Analysis of variance (ANOVA) is applied to identify the most significant operating parameters. Methylene blue (MB) adsorption and toxicity leaching test of biochar are also carried out to assess the pore adsorption ability and heavy metal retention potential, with results provided in Appendix C and D. Comparisons between the yield and pore properties of biochar derived from conventional pyrolysis of RDF and MACP of sawdust are also performed to understand the influence of different heating methods and feedstock on biochar quality.

4.1 Effect of catalysts on biochar yield and properties

4.1.1 Biochar yield

Biochar yield (Y_b) is calculated using the following equation:

$$Y_b = \frac{m_b}{m_{RDF}} \times 100\% \tag{4.1}$$

In which m_b refers to the weight of solid residues recovered on the filter after filtration (removing soluble catalysts and chemicals) and drying (removing moisture), m_{RDF} is the weight of dry RDF feedstock (10g). Results are reported as the average of triplicate tests.

Figure 4.1 illustrates the yield of biochar produced from MACP of RDF and sawdust using different catalysts, as well as from conventional pyrolysis of RDF using 20 wt.% K_2CO_3+10 wt.% bentonite. The yield of RDF derived biochar was around 15%, whereas the yield of sawdust derived biochar was 27%, probably because sawdust has less volatile content and more fixed

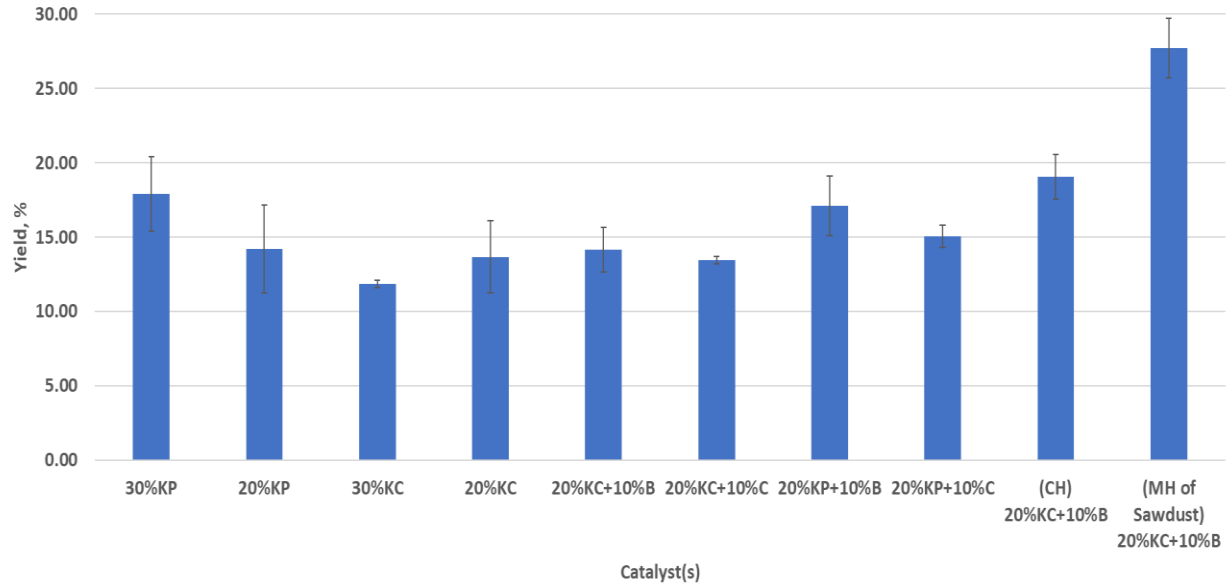

Figure 4.1 Yield of biochar produced from MACP and conventional pyrolysis of RDF and MACP of sawdust mixed with different catalysts under 1200 W microwave power, 550 °C final temperature and 30 min microwave radiation time (%: wt.%, KP: K_3PO_4, KC: K_2CO_3, B: bentonite, C: clinoptilolite, CH: conventional heating, MH: microwave heating).

carbon content than RDF (Table 4.1). Because of very low heating rate (30 °C/min), biochar yield from conventional pyrolysis was slightly higher than MACP of RDF. In MACP of RDF using single catalyst, biochar yield decreased with increasing K_2CO_3 content from 20 wt.% to 30 wt.% at a corresponding heating rate decrease from 184 °C/min to 82°C/min. K_3PO_4 showed a trend opposite to K_2CO_3 in terms of the relationship between heating rate and biochar yield. For the cases with two catalysts, bentonite promoted biochar production more than clinoptilolite. Compared with single catalyst, there was only slight increase of biochar yield for catalyst mixtures, and biochar yield of 20 wt.% K_2CO_3+10 wt.% clinoptilolite was almost the same as 20 wt.% K_2CO_3. The largest increase was caused by 20 wt.% K_3PO_4+10 wt.% bentonite. Overall, 30 wt.% K_3PO_4 had the highest biochar yield among all catalyst cases in MACP of RDF, which was also reported by Mohamed et al. (2016b) in MACP of switchgrass.

Under the same microwave power, pyrolysis temperature and time, biochar yield mainly depends on heating rate and particle size (Spokas et al., 2012). For catalytic pyrolysis, heating rate is determined by the dielectric properties of catalyst, while the RDF sample is quite heterogeneous, which results in a non-uniformly distributed mixture of feedstock and catalyst particles in the reactor. For 30 wt.% K_2CO_3, although the heating rate is similar to 30 wt.% K_3PO_4, RDF sample in regions with high K_2CO_3 concentrations will react first, leading to the formation of biochar and even decomposition of some K_2CO_3 as mentioned in section 3.3.1. This brings out the possibility that regions without K_2CO_3 may not have the opportunity to undergo pyrolysis reactions and become "dead-zones". A large number of "dead-zones" were found after MACP of RDF using 30 wt.% K_2CO_3. On the other hand, K_3PO_4 is much more stable than K_2CO_3 and could act as a heat transfer media throughout the whole pyrolysis process, resulting in the formation of more biochar.

Benefiting from their porous structures, bentonite and clinoptilolite exhibit a noteworthy catalytic effect on secondary tar cracking reactions and thus improved bio-oil yield (Pütun et al., 2009). According to the results shown in Figure 4.1, biochar yield is mostly determined by the catalytic effect of main catalyst. On the other hand, bentonite performs better than clinoptilolite in terms of improving biochar yield. This may be because that clinoptilolite has an outstanding performance in promoting the formation of bio-oil than other natural zeolites which results in a relatively low biochar yield (Park et al., 1999).

Compared with the char yield (23%) obtained at 500 °C in conventional pyrolysis of RDF from Cozzani et al. (1995a), our results prove that the yield of biochar produced from pyrolysis of RDF is quite low, no matter whether under conventional heating or microwave heating. Due to the high

volatile content in RDF, the use of different heating method and catalyst may not have a significant impact on biochar yield, but the increase in heating rate and catalytic vapour cracking may benefit the creation of porous structures in biochar, thus improving its pore properties and quality (Bridgwater, 2012; Luque et al., 2012). It should be noted that the actual biochar yield is expected to be up to 5% (~0.5 g) higher than the currently reported value, due to the potential biochar loss in the collection, filtration and drying process. The lost biochar particles are either sticking to the quartz tube and filter, or in the leachates which is difficult to be recovered.

4.1.2 Biochar compositions

Table 4.1 shows the compositions of RDF, sawdust and biochars produced from MACP of RDF using different catalysts, based on proximate and ultimate analyses. The ash content of biochar refers to the original inorganic matter in RDF feedstock and residual catalyst that is not totally removed by filtration after pyrolysis. As expected, the volatile content in RDF sample was very high (90%), whereas ash and fixed carbon content was low at approximate 5%. After pyrolysis, for biochar produced with single potassium catalyst, the ash content was about 30%, with the highest of 33% recorded for 20 wt.% K_3PO_4. For biochar produced with combined catalysts, the ash content increased to about 50%, probably because the final solids product contains high amount of bentonite and clinoptilolite which have poor solubility in distilled water. Fixed carbon content of biochar increased from 5% for RDF to 40% for single potassium catalyst and 30% for combined catalyst, but volatile content decreased dramatically.

Table 4.1 Compositions of pre-dried RDF, sawdust feedstock and biochar samples produced from MACP of RDF mixed with different catalysts (unit: wt.%).

Sample	Ash	Volatile	Fixed carbon[a]	C	H	O[a]	N	C[b]	H[b]	O[b]	N[b]
20%KP	33.23	21.64	45.13	55.35	1.99	8.81	0.63	82.89	2.98	13.19	0.94
30%KP	27.22	31.26	41.52	57.61	2.81	11.80	0.56	79.15	3.86	16.22	0.77
20%KC	27.69	31.70	40.61	54.43	2.73	14.39	0.77	75.27	3.77	19.91	1.06
30%KC	24.90	35.26	39.84	57.51	3.55	13.30	0.74	76.57	4.73	17.72	0.99
20%KP+10%B	50.45	22.33	27.22	34.47	1.54	13.20	0.34	69.56	3.11	26.64	0.69
20%KP+10%C	48.39	19.01	32.60	40.91	1.63	8.71	0.37	79.25	3.16	16.88	0.71
20%KC+10%B	45.27	29.61	25.12	40.66	2.08	11.59	0.41	74.28	3.80	21.17	0.75
20%KC+10%C	52.34	21.71	25.95	37.29	1.42	8.43	0.53	78.24	2.97	17.69	1.10
RDF	5.03	90.42	4.55	58.85	7.27	27.63	1.22	61.97	7.66	29.09	1.28
Sawdust	0.76	77.01	22.53	48.52	6.39	44.65	0.13	48.67	6.41	44.79	0.13

a: calculated by difference; b: dry ash free basis.

Table 4.2 Elemental composition of original biochar samples (i.e. without catalyst separation) produced from MACP of RDF mixed with different catalysts by ICP-AES analysis.

Sample	%				mg/kg (ppm)							
	K	P	Mg	Ca	Fe	Cu	Zn	Sn	Mn	Cr	Cd	Pb
20%KP	12.24	3.33	0.07	0.60	451.89	7.69	162.13	22.43	8.43	3.85	0.49	14.68
20%KC	11.56	0.05	0.07	0.55	490.31	9.40	99.13	21.49	8.38	3.44	0.66	25.99
20%KP+10%C	10.82	2.67	0.06	0.52	972.38	6.93	75.83	10.01	22.97	2.08	0.57	7.82
20%KC+10%B	10.25	0.05	0.20	0.57	0.22(%)	6.94	114.82	19.89	13.90	3.56	1.04	23.44

Given the 5% ash content in RDF and 15% biochar yield, if we assume that all ash in RDF feedstock will remain in the biochar product after pyrolysis, the ash content is expected to be 33% in the biochar sample. For K_2CO_3 and 30 wt.% K_3PO_4, the ash content of collected biochar was found to be below 33%, which can be attributed to the loss of ash during pyrolysis, either being carried away by the gases or failed to be collected. As fine ash particles may block the pores in biochar, less ash content in biochar means higher porosity of the biochar. When bentonite and clinoptilolite were tested, the ash content of biochar increased by 20 %, which lowered the fixed carbon content of biochar and consequently a lower biochar specific surface area.

C, H, O and N content were obtained from ultimate analysis. Compared to RDF, the hydrogen and oxygen content in biochar were much lower, whereas carbon content remained the same for single potassium catalyst but reduced for combined catalysts, mainly because of the high ash content. Biochar produced with K_2CO_3 had a higher oxygen content than that with K_3PO_4, probably as a result of the "dead-zones" found in K_2CO_3 cases. On an ash-free basis, the carbon content of the biochar could reach more than 80%. Combined with changes of volatile and fixed carbon content, all results suggest that most of the H and O containing functional groups have decomposed and removed, with carbon content being increased compared to RDF after pyrolysis. It could also be inferred that water vapour and light hydrocarbons released from the interior region of RDF particles and creates various channels, leading to the formation of the porous structure of biochars.

Some representative samples were selected for quantifying the content of essential plant nutrients (K, P, Mg, Ca), micronutrients (Fe, Cu, Zn, Sn, Mn) and heavy metals (Cr, Cd, Pd) for soil applications, with results given in Table 4.2. Micronutrients are beneficial for plant growth and for

improving soil fertility, whereas the heavy metal content should be controlled in a tolerable range (Mullen et al., 2010). These four samples shared similar K, Mg and Ca contents and 20 wt.% K_3PO_4 and 20 wt.% K_3PO_4+10 wt.% clinoptilolite had higher P content because of the addition of K_3PO_4 catalyst. A noticeable increase was found in Fe and Mn contents after adding bentonite and clinoptilolite, because natural clays and zeolites contain iron and magnesium, especially for bentonite in which one of the main ingredients is iron oxide (Khoeini et al., 2009). All heavy metal contents reported in Table 4.2 are below the threshold value limited for soil of agricultural purpose, according to the Canadian Soil Quality Guidelines listed in Table 4.3 (CCME, 2007). This means that those biochars can be safely applied to agricultural soil.

Table 4.3 Canadian Soil Quality Guidelines for agricultural soil.

Substance	Cr	Cd	Pb	Cu	Zn
Threshold value (mg/kg)	64	1.4	70	63	200

4.1.3 Pore properties

Biochar pore properties, including specific surface area, average pore diameter, micropore area and volume, pore size distribution and pore morphology, are important parameters to characterize the biochar quality, especially for its adsorption abilities. Table 4.4 summarizes the pore properties of biochar produced from microwave and conventional pyrolysis of RDF using different catalysts, as well as from MACP of sawdust. The average heating rate of each case has also been indicated to infer possible relationship between pore properties and reaction heating rate. Several findings can be drawn from those data: (1) In MACP of RDF, BET surface area of biochar produced from 30 wt.% K_2CO_3 was the highest (285.6 m^2/g), followed by 20 wt.% K_2CO_3 + 10 wt.% bentonite

Table 4.4 BET surface area, average pore diameter, micropore area and pore volume of biochar produced from MACP of RDF, conventional heating of RDF (CH) and MACP of sawdust (SD) using different catalysts under 1200 W microwave power, 550 °C final temperature and 30 min microwave radiation time.

Biochar type	Heating rate (°C/min)	BET surface area (m^2/g)	Average diameter (nm)	Micropore area (m^2/g)	Pore volume (cm^3/g)
20%KC	184	156.0±1.5	4.80	80.3	0.037
20%KP	115	66.4±0.7	5.48	-	-
30%KC	82	285.6±2.9	5.00	153.4	0.070
30%KP	57	104.0±0.7	6.85	-	-
20%KC+10%B	163	205.8±2.6	4.86	130.7	0.060
20%KP+10%B	167	74.4±1.3	5.92	-	-
20%KC+10%C	173	125.0±1.0	5.15	55.3	0.025
20%KP+10%C	181	54.3±0.7	6.14	-	-
(CH) 20%KC+10%B	20	60.2±1.7	5.48	-	-
(SD) 20%KC+10%B	174	358.0±4.4	4.16	229.4	0.106

(205.8 m^2/g) and 20 wt.% K_2CO_3 (156.0 m^2/g); (2) For single catalyst, the surface area of biochar produced from K_2CO_3 was much higher than that of K_3PO_4, and increasing mixing ratio from 20 wt.% to 30 wt.% increased biochar surface area for both K_2CO_3 and K_3PO_4; (3) Adding bentonite to potassium catalyst was beneficial for increasing biochar surface area, but opposite was observed for clinoptilolite; (4) MACP of RDF produced biochars of much higher surface area than from conventional pyrolysis of RDF (60.2 m^2/g), which confirmed that microwave heating could create more porous structure in biochar; (5) There were large differences between the surface area of biochar produced from MACP of sawdust and RDF, with RDF-derived biochar having much lower surface area. This is probably because of the high O content in sawdust which evaporates mainly in the form of H_2O and CO_2, leading to the formation of more pores; (6) The average diameter of

produced biochar was similar for all samples at about 5 nm; (7) The micropore area and pore volume were positively correlated with BET surface area and could not be detected if the BET surface area was too low (< 125 m^2/g) or average pore diameter was too high (> 5.15 nm), due to instrument limitation.

In view of the strong relationship between heating rate and biochar surface area, it was recognized that physical properties of biochar produced from fast pyrolysis at high heating rate should be quite different from that from slow pyrolysis at low heating rate (Luque et al., 2012). A higher heating rate in pyrolysis is expected to promote the removal of moisture and organic compounds from the interior of particles, favoring the destruction of cell walls and formation of large size pores in biochar (Cetin et al., 2004; Mohamed et al., 2016b). This contributes to the formation of more large pores (mesopores and macropores), whereas it may reduce the amount of micropores, and thus affects total surface area (Liu et al., 2012). In this study, microwave heating with much higher heating rate produced biochar with much higher specific surface area than conventional heating. However, there appears to be no clear relationship between heating rate and specific surface area in MACP of RDF, especially when focusing on the high heating rate but low specific surface area of biochar produced from 20 wt.% K_3PO_4, which is likely because the catalyst reactivity and load ratio play a dominant role in creating porosity in biochar.

The reactivity and stability of K_2CO_3 and K_3PO_4 are quite different during MACP of RDF. K_2CO_3 was regarded as a suitable activator to produce activated carbon with high surface area under microwave irradiation in many previous researches (Foo and Hameed, 2012b; Nowicki et al., 2016; Okman et al., 2014; Shang et al., 2015; Tay et al., 2009). According to Eqs. (3.1) and (3.2),

K, K_2O, CO and CO_2 formed under inert atmosphere during heating may diffuse in or out the char matrix, causing more porous structures and enlarging pore size, which is favorable for improving specific surface area (Foo and Hameed, 2011). K_3PO_4 remains stable during pyrolysis, not contributing to the activation of biochar. Increasing catalyst load will strengthen the char activation for K_2CO_3 and efficiency of microwave absorption for both K_2CO_3 and K_3PO_4, hence increasing specific surface area. When catalyst mixtures were used, the heating rate was similar, but the specific surface area varied significantly. Bentonite could promote exothermic reactions and inhibit the endothermic reactions between C and CO_2 because of the presence of iron and cadmium (Sulman et al., 2009; Zhao et al., 2014). This will accelerate heating and result in faster decomposition reactions and porosity formation, thus increasing the surface area. Clinoptilolite is favorable for increasing heating rate if mixed with K_3PO_4. On the other hand, most of clinoptilolite will remain in the solid residue with biochar and ash because of its high stability during pyrolysis and low water solubility. Consequently, clinoptilolite may not contribute to the creation of surface area and pore volume.

SEM images of biochar produced from MACP of RDF using 20 wt.% K_2CO_3, 20 wt.% K_3PO_4 and 20 wt.% K_2CO_3 + 10 wt.% bentonite were taken to understand the surface morphology. As shown in Figure 4.2, the surface topography of biochar produced from K_2CO_3 and K_3PO_4 differs significantly. The surface was very smooth and full of cavities and channels for biochar produced from K_2CO_3, but was quite rough without any clear pore outlines for biochar produced from K_3PO_4. These pores are believed to result from the diffusion of volatile compounds and gases created from decomposition of K_2CO_3.

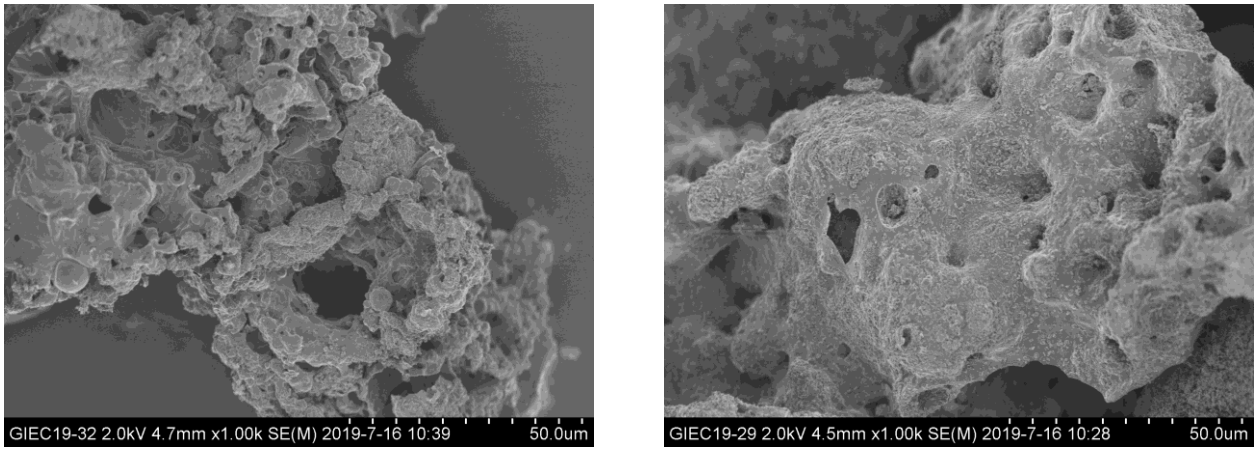

20% K_2CO_3

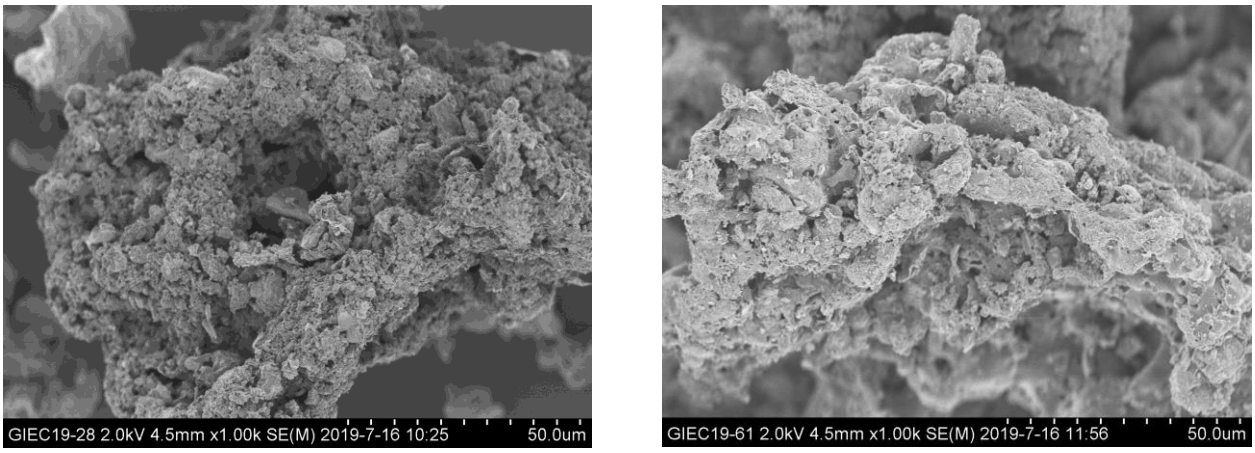

20% K_3PO_4

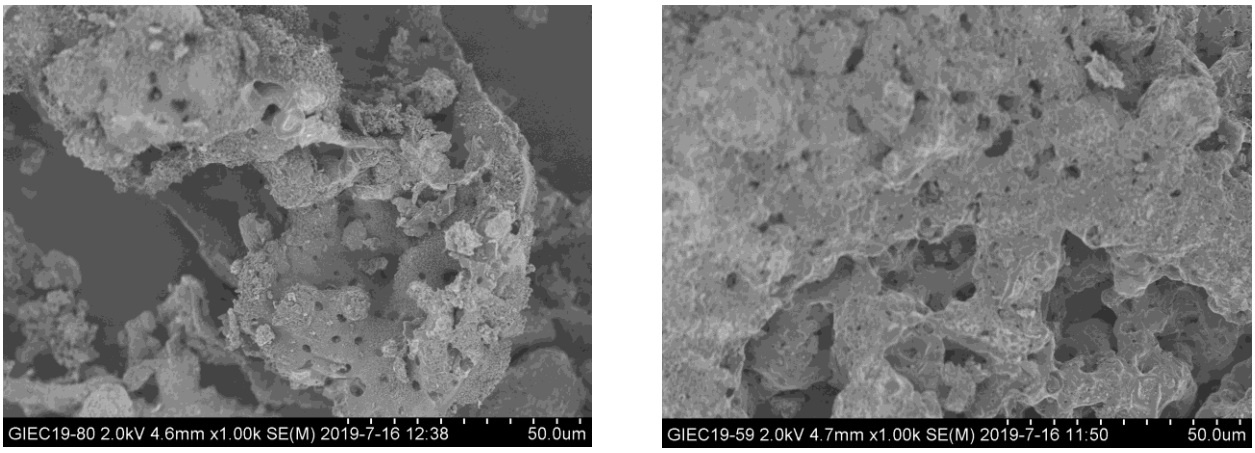

20% K_2CO_3 + 10% bentonite

Figure 4.2 SEM micrographs of biochar samples produced from MACP of RDF mixed with 20 wt.% K_2CO_3, 20 wt.% K_3PO_4 and 20 wt.% K_2CO_3 +10 wt.% bentonite under 1200 W microwave power, 550 °C final temperature and 30 min microwave radiation time.

According to the classification of IUPAC-pore dimensions, various pores in adsorbents could be classified into micropores (d<20 Å), mesopores (d=20-500 Å) and macropores (d>500 Å). Pore size distribution is of great importance in determining the fraction of total pore volume accessible to molecules of certain size. Figure 4.3 depicts the pore size distribution of biochar samples produced from different feedstock, catalysts and heating methods obtained by applying standard BJH methods. Together with data shown in Table 4.4, it is seen that micropores were not detected in biochars produced from 20 wt.% K_3PO_4 and conventional pyrolysis of RDF, indicating that micropore volume was very low in those two samples. For other four samples, the pore volume of biochar samples increased markedly in micropore region. The highest micropore volume was recorded for biochar produced from MACP of sawdust, followed by MACP of RDF using 30 wt.% K_2CO_3, 20 wt.% K_2CO_3 + 10 wt.% bentonite and 20 wt.% K_2CO_3, which followed the same order as their BET surface area. It seems that micropores contribute the most to the surface area of

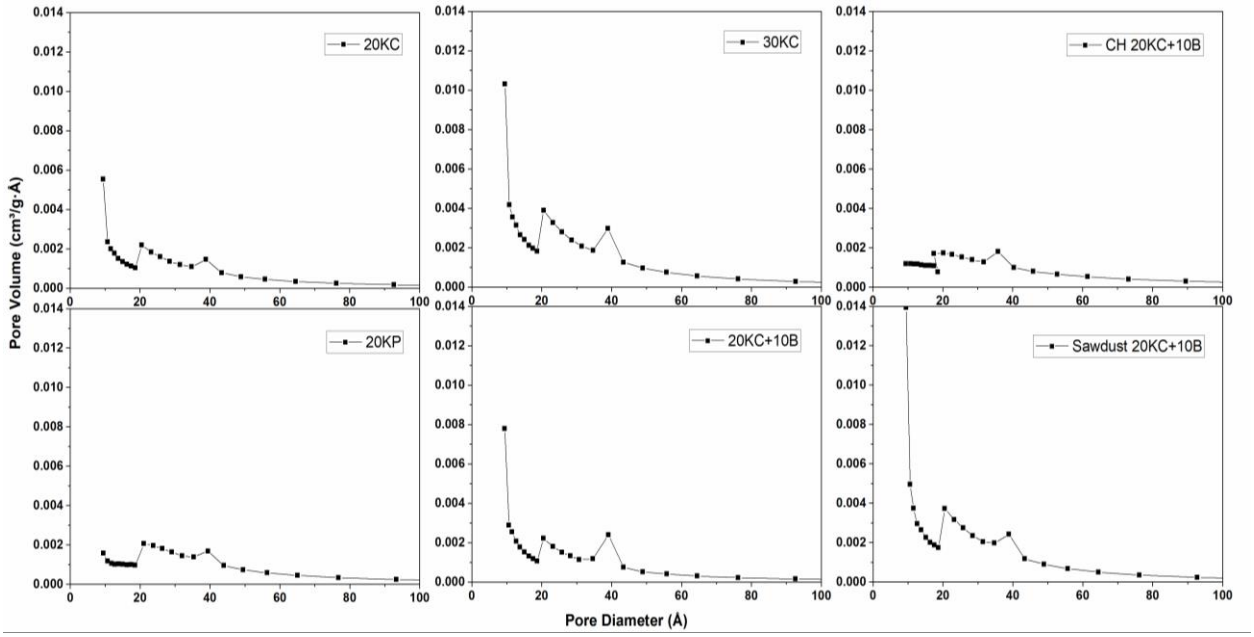

Figure 4.3 Pore size distribution of biochar samples produced from conventional pyrolysis of RDF, MACP of RDF and MACP of sawdust mixed with different catalysts under 1200 W microwave power, 550 °C final temperature and 30 min microwave radiation time (1 Å=0.1 nm).

biochar and are responsible for the high adsorptive capacity for small molecules. The figure also shows the development of mesopore volume. For all samples, there is a peak around 40 Å in the mesopore range, and the mesopore volume increases following a similar trend as micropore volume. It could be inferred that together with micropores, large quantities of mesopores were also generated in MACP of RDF and sawdust when K_2CO_3 was used as catalyst, and increasing K_2CO_3 load or adding bentonite was also beneficial for creating mesopores and micropores.

In general, adsorption performance of biochar depends on both the pore structure and functional groups, as well as adsorbates. Based on the adsorption free energy and molecular collision theory, adsorbates are preferentially adsorbed in pores of size similar to the adsorbate molecular size due to the greater number of contact points between pores and adsorbates (Pelekani and Snoeyink, 1999). Micropores and mesopores will have specific applications for adsorbates of different diameters. For example, micropores are suitable for adsorbing smaller molecules such as iodine atoms (d=2.7 Å) which can easily penetrate into micropores larger than 10 Å, whereas some of the large micropores and most of the mesopores are responsible for methylene blue (MB) adsorption (Baçaoui et al., 2001). The minimum cross-section of MB molecule is estimated to be about 8 Å, whereas the minimum pore diameter it can enter is 13 Å (Barton, 1987). A preliminary tests of biochars on MB adsorption were conducted in this study, with results given in Appendix C. Because of lockdown of research labs during COVID-19 pandemic, the reproducibility of data was not checked and thus caution should be exercised in interpreting those data.

4.1.4 Functional groups

Fourier transform infrared spectroscopy (FTIR) were obtained in Figure 4.4 to identify the surface functional groups. It is seen that there exist similar peaks in absorbance bands among all six biochar samples. According to previous FTIR studies on carbon materials (Aguilar et al., 2003; Boonamnuayvitaya et al., 2005; Deng et al., 2010; Zhuang et al., 2019), the band at 3421 cm^{-1} is attributed to O-H stretching of hydroxyl groups, which is strong for 20KC+10C. The band at 3178 cm^{-1} is attributed to C-H stretching in aromatic compounds, but it is as weak as that of O-H stretching. Except for samples with 20KP and 20KC+10B, the small peak at 2924 cm^{-1} with its small shoulder at 2850 cm^{-1} in other four samples are ascribable to C-H stretching originating from methyl and methylene groups that is usually contained in organic matters. The overlap peaks around 1700 cm^{-1} (1650-1720 cm^{-1}) are ascribed to C=O stretching (saturated ketone and lactone

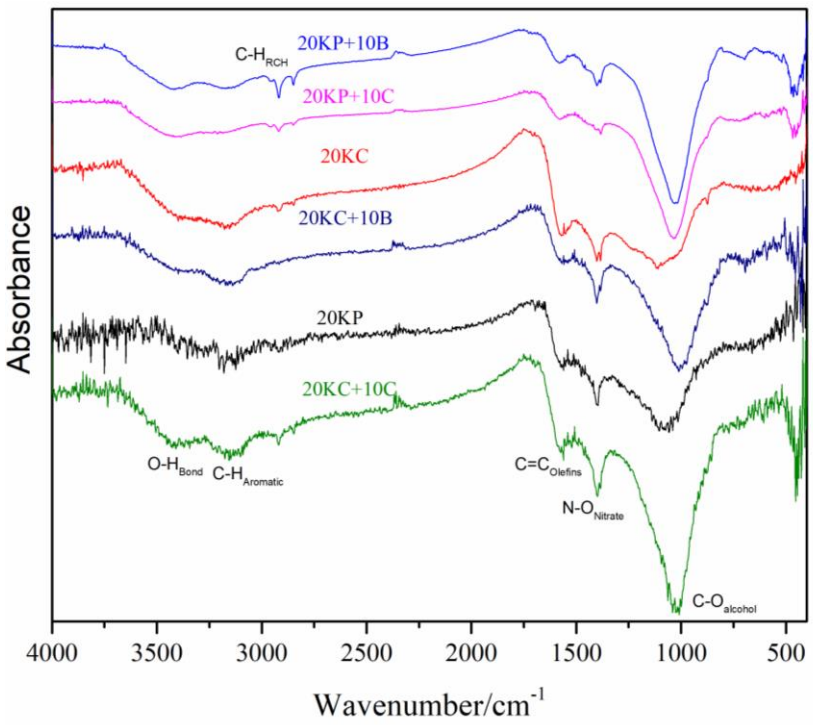

Figure 4.4 FTIR spectra of biochar samples produced from MACP of RDF mixed with different catalysts under 1200 W microwave power, 550 °C final temperature and 30 min microwave radiation time.

carbonyl, carboxylates) and likely C=C stretching in olefins or aromatic rings. There is also a marked peak at 1384 cm^{-1} which represents nitrate in solid waste samples. With an intensive peak at around 1100 cm^{-1}, the most sufficient absorption takes place which symbolizes the existence of C-O stretching (1000-1300 cm^{-1}), normally included in ethanol, ether, phenol, etc. The intensity of C=O, C=C and N-O stretching is similar among these six samples, but for C-O stretching, a very strong absorption for 20KC+10C and a relatively weak band for 20KC and 20 KP are observed, probably due to the added bentonite and clinoptilolite remaining in the biochar sample. The criteria on determining functional groups in FTIR could be found in Appendix B.

After MACP of RDF, very few aromatic compounds remain in the produced biochar. The aromatic compounds originate from lignin in wood and paper which composes about 30% of RDF. It is found that most complex aromatic compounds break down and evaporate during pyrolysis, resulting in a highly carbonized char. The high intensity of C-O stretching in alcohols is not favorable for producing graphitic coke but oxygenated coke. The oxygen content in the biochar is higher than expected, as shown in Table 4.1. The most useful functional groups for chemisorption under general circumstances are the hydroxyl groups, which possess a strong polarity and ability in linking with other polar molecules, but unfortunately only few hydroxyl groups are identified in those samples. The catalyst type does not show a significant impact on the formation of different functional groups in the produced biochar from MACP of RDF.

4.2 Effect of microwave power intensity on biochar yield and pore properties

Previous results showed that the surface area of biochar produced from MACP of RDF mixed with 20 wt.% K_2CO_3 + 10 wt.% bentonite was higher than other catalyst cases, except for 30 wt.%

K_2CO_3. However, from the economics point of view, 20 wt.% K_2CO_3 + 10 wt.% bentonite may be better than 30 wt.% K_2CO_3. Therefore, 20 wt.% K_2CO_3 + 10 wt.% bentonite was selected as the optimum case for further investigation on the effect of operating conditions on biochar yield and pore properties, especially on the specific surface area and pore morphology. The analysis of variance (ANOVA) method is applied to analyze the dependence of specific surface area and biochar yield on different operating conditions, including microwave power input, targeted pyrolysis temperature and microwave radiation time.

According to Table 3.3, there was a positive correlation between microwave power and heating rate. Thus, by adjusting microwave power using the same catalyst in MACP of RDF, the dependency of yield and surface area of biochar on heating rate can be investigated. The biochar surface area and yield as a function of heating rate are plotted in Figure 4.5 together with standard error bars and trendlines. The biochar surface area was low at 30 ºC/min heating rate (700 W microwave power), and steadily increased to a maximum of 225 m^2/g with the increase of heating rate before it dropped slightly afterward. The errors at 800, 900 and 1100 W microwave power were quite large, likely due to the heterogeneity of RDF sample and experimental errors. Clearly, too low a heating rate is not beneficial for producing biochar with higher specific surface area, but too high a heating rate also does not result in further improvement of biochar porosity. In this study, 1000 W microwave power appeared to be the optimum. On the other hand, based on Figure 4.5(b), there is not a clear relationship between heating rate and biochar yield in MACP of RDF, with the values ranging from 14% to 19%. Although many researchers reported that higher heating rate typically results in a lower biochar yield in pyrolysis of biomass, the heterogeneity of RDF brings about difficulties on finding a general trend between biochar yield and heating rate.

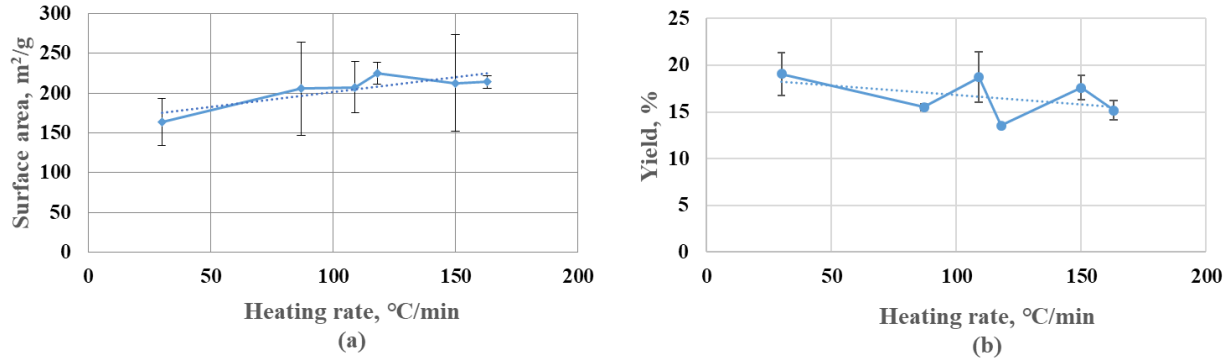

Figure 4.5 (a) surface area and (b) yield of biochar produced by MACP of RDF mixed with 20% K_2CO_3 + 10% bentonite under different microwave power (heating rate), 550 °C final temperature and 30 min microwave radiation time.

One-way ANOVA analysis was applied on biochar surface area and yield against heating rate, with microwave power varied from 700 W to 1200 W. Usually, the larger the F value, the greater dependence of the dependent variables (biochar surface area and yield) on the independent variables (microwave power intensity). There will be a statistically significant difference in the mean values of dependent variables if the significance (Sig.) is below 0.05. Table 4.5 showed that there was not a statistically significant difference between groups of biochar surface area and yield under different microwave power intensity, as indicated by low F values and high p values. The F

Table 4.5 One-way ANOVA of biochar surface area and yield under different microwave power intensity.

Biochar parameter		Sum of squares	Degree of freedom	Mean square	F	Sig. (*p*)
Surface area (at different heating rate)	Between groups	4245	5	849.1	0.22	0.94
	Within groups	23406	6	3901.0		
	Total	27651	11			
Yield (at different heating rate)	Between groups	47.9	5	9.582	1.88	0.23
	Within groups	30.5	6	5.085		
	Total	78.4	11			

value for biochar yield was larger than that for surface area, which indicates that the heating rate (microwave power intensity) may have a greater effect on biochar yield than on surface area.

4.3 Effect of temperature and time on biochar yield and surface area

Pyrolysis temperature and microwave radiation time are two important operating parameters influencing pore properties and yield of biochar produced by MACP of RDF, which are investigated using RDF mixed with 20 wt.% K_2CO_3 + 10 wt.% bentonite under 1000 W microwave power input in this study. As shown in Figure 4.6, specific surface area of biochar produced at 400 ºC was low (135 m^2/g) and increased to a maximum of 264 m^2/g when pyrolysis temperature reached 500 ºC, before dropped down afterward. On the other hand, biochar yield decreased with the increase of temperature from 400 ºC to 500 ºC and remained constant after that. With the increase of time, biochar surface area increased first and reached the highest at 30 mins, and then fell to below 200 m^2/g when the time became 60 mins or longer. Biochar yield decreased slightly and remained constant after 60 mins. It is worth to point out that the specific surface area of biochar produced at 500 ºC in 30 minutes is always the highest in both cases.

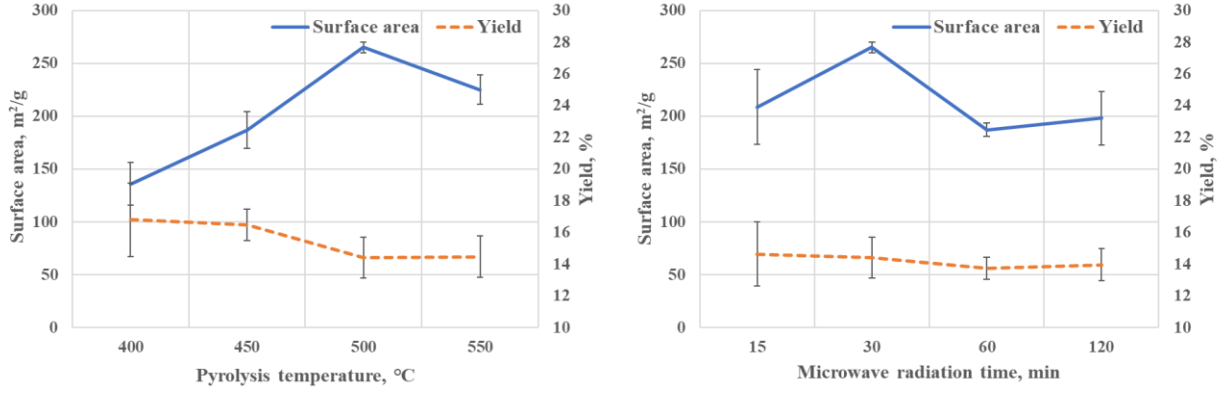

Figure 4.6 (a) Specific surface area and (b) yield of biochar produced by MACP of RDF mixed with 20% K_2CO_3 + 10% bentonite under 1000 W microwave power, different targeted pyrolysis temperature (microwave radiation time: 30 min) or microwave radiation time (pyrolysis temperature: 500 ºC).

Biochar pore properties, including specific surface area, pore size, etc., are significantly influenced by pyrolysis temperatures (Cheng and Li, 2018). Understandably, a high temperature could widen pores because it destroys the walls between adjacent pores, causing the enlargement of pores. Meanwhile, as temperature rises, more volatiles are expected to be released from bulk surface and inner matrix of biomass, which creates a larger surface area and more porous structure (Liu et al., 2015; Zhao et al., 2018). However, too high a temperature (T> 600 ºC) may promote the fusion of pores (Muradov et al., 2012), which tends to destroy microporous structures and generates more mesopores and macropores, thus lowering the total surface area to some extent. This could explain that the optimum pyrolysis temperature was found to be around 500 ºC for MACP of RDF. Pyrolysis temperature also has a great influence on biochar yield. With the increase of temperature from 200 ºC to 800 ºC or ever higher, char yield will decrease for most of biomass feedstock (Menéndez et al., 2007). The influence of temperature on char yield is more significant at lower temperature regions than at higher temperature regions (Zhao et al., 2018). In this study, higher temperature benefits the release of volatiles in RDF and consequently less amount of solid residues remains. However, when temperature reaches 500 ºC or higher, most of the volatiles has broken down and evaporated, which means that the solid yield will remain constant. This is in consistence with TGA results in Figure 3.1.

Biochar surface area and yield are also influenced by microwave radiation time. It took about 8 mins to reach targeted temperature or steady state for cases with the same catalyst and microwave power intensity, as shown in Figure 4.6. For a total microwave radiation time of 15 mins, the residence time at targeted temperature was very short at 7 mins. Nevertheless, the surface area still reached above 200 m^2/g. One explanation is that the biochar surface area is mainly enlarged by

cracking reactions over a relatively short period after hotspot appears, which creates most of the pores in biochar matrix. It could be assumed that most of the pores have formed at around 30 mins microwave radiation time, whereas much longer time may destroy porous structures, resulting in the drop of surface area to approximately 200 m^2/g. Similar to the effect of temperature on biochar surface area, too long a residence time also has an adverse effect on decreasing the biochar surface area. With regard to biochar yield, it seems that all cracking reactions have completed at around 60 mins. The steady decrease of biochar yield is expected as more volatiles are expected to be released over longer residence time. Similar results on effects of residence time on specific surface area and yield of rapeseed stem derived biochar can be found in Zhao et al. (2018).

One-way ANOVA was applied to determine the impact of pyrolysis temperature and microwave radiation time on biochar surface area and yield, with the results given in Table 4.6. The largest F value (26.0) with significance $p< 0.001$ was found between temperature and surface area, followed by time and surface area ($F=4.86$, $p=0.033$). It indicated that there was a significant difference in biochar surface area between groups of data at different pyrolysis temperature and a moderate difference in biochar surface area between groups of data at different microwave radiation time. There were not huge impacts of targeted pyrolysis temperature and microwave radiation time on biochar yield ($p> 0.05$). The same ANOVA results were reported by Zhao et al. (2018).

The pore morphology of biochar produced at different targeted pyrolysis temperature and microwave radiation time are shown in Figure 4.7. For biochar produced at 400 ºC, pore structures had not yet fully developed and visible pores could be hardly observed on the biochar surface. With the increase of temperature to 500 ºC, more and more porous channels with explicit outlines

were generated and the gap between pores narrowed down. This indicates more destructions of cell walls and fusion of pores in solid matrix with the increase of pyrolysis temperature. The shape and distribution of pores evolve from the carbonaceous skeleton of capillary structure of lignocellulosic feedstock (Zhang et al., 2015). Biochar produced at 15 mins microwave radiation time shared similar results with that at 400 ºC. With the extension of time, especially beyond 60 mins, pores fused severely in association with a large jump in pore size, which was not favored for creating more micropores and improving the total surface area.

Table 4.6 One-way ANOVA of biochar surface area and yield under different targeted pyrolysis temperature or microwave radiation time.

Parameter		Sum of squares	Degree of freedom	Mean square	F	Sig. (*p*)
Surface area (at different temperature)	Between groups	27308	3	9102	26.018	0.000
	Within groups	2798	8	349		
	Total	30107	11			
Yield (at different temperature)	Between groups	14.693	3	4.898	1.352	0.325
	Within groups	28.973	8	3.622		
	Total	43.667	11			
Surface area (at different time)	Between groups	10809	3	3603	4.861	0.033
	Within groups	5929	8	741		
	Total	16738	11			
Yield (at different time)	Between groups	1.497	3	0.499	0.184	0.904
	Within groups	21.660	8	2.708		
	Total	23.157	11			

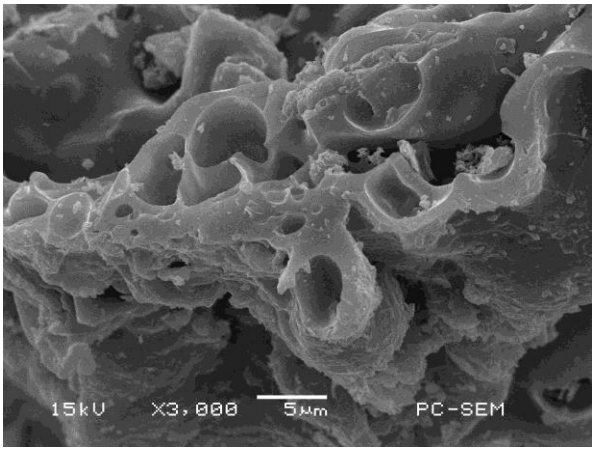

400 ºC, 30 mins

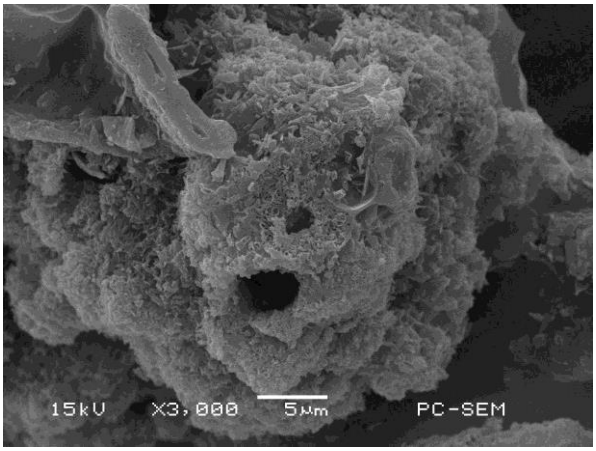

500 ºC, 15 mins

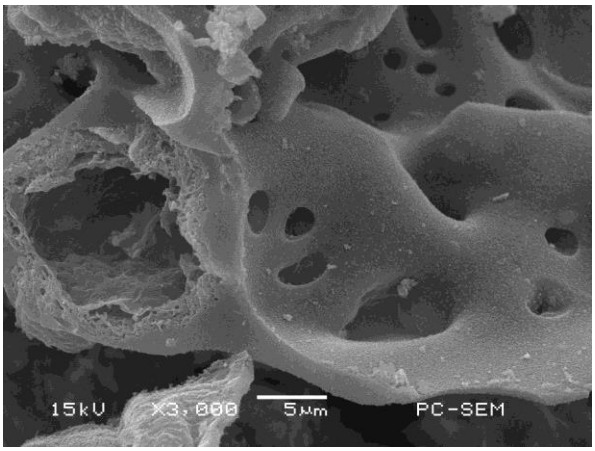

450 ºC, 30 mins

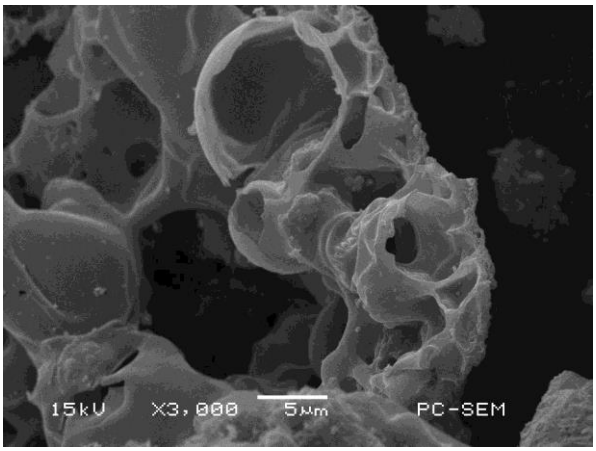

500 ºC, 60 mins

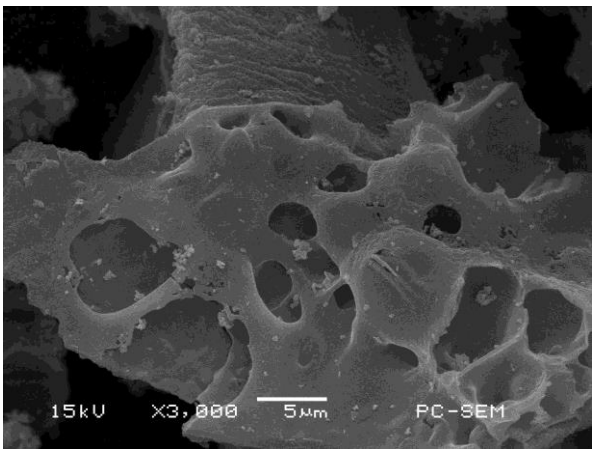

500 ºC, 30 mins

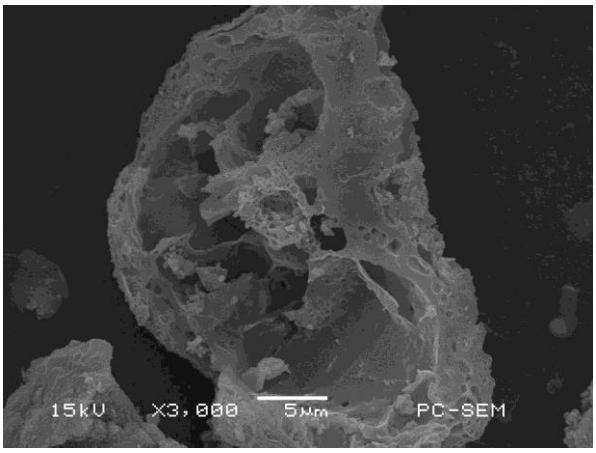

500 ºC, 120 mins

Figure 4.7 SEM micrographs of biochar samples produced from MACP of RDF mixed with 20% K_2CO_3 + 10% bentonite under 1000 W microwave power with different pyrolysis temperature and microwave radiation time.

4.4 Summary

Biochar produced from MACP of RDF using different catalysts shares varied results of proximate and ultimate analysis, pore properties and MB adsorption application performance, but similar yield and functional groups. Biochar yield is around 15% and varies in ±5% with different catalysts. The low yield is probably due to high ash and volatile content in RDF and difficulty of recovering biochar sample in further treatments after MACP. It is supposed that large groups of light volatiles decompose and evaporate, with the carbon content enriched during MACP, causing porous structures of biochar. K_2CO_3 is a very effective catalyst, not only accelerates heating rate, but also helps produce biochar with higher surface area and more micro and mesopores, which is beneficial for MB adsorption. Biochar produced by different catalysts have respective advantages, e.g., 30 wt.% K_2CO_3 is suitable for adsorption applications; 20 wt.% K_2CO_3 + 10 wt.% bentonite is cost effective with high surface area of biochar; K_3PO_4 may be beneficial for plant growth and heavy metal adsorption.

Based on statistical analysis, there is no significant impact of heating rate (microwave power intensity) on biochar surface area and yield. However, the targeted pyrolysis temperature is the most influential parameter affecting biochar surface area, followed by microwave radiation time. Reasonably, biochar yield has a negative correlation with pyrolysis temperature and microwave radiation time. For biochar produced by MACP of RDF mixed with 20 wt.% K_2CO_3 + 10 wt.% bentonite, 1000 W microwave power, 500 ℃ targeted pyrolysis temperature and 30 minutes microwave radiation time are the optimum operating conditions.

Chapter 5: Conclusions and future work

Increasing generation and accumulation of solid waste raise ecological and environmental issues worldwide. With increasing concern about proper disposal of solid waste, researchers have been exploring new ways to handle municipal wastes ranging from reduction, reuse and recycling. One approach is to pretreat heterogeneous and wet combustible solid wastes and make them into refuse-derive fuel (RDF) which is suitable for further thermochemical conversions, such as combustion, gasification or pyrolysis to produce heat, power or value-added products. In pyrolysis, biochar is produced as a byproduct, which can be applied for repairing contaminated soil. However, biochar derived from conventional pyrolysis of RDF has a poor quality. In this study, microwave-assisted catalytic pyrolysis (MACP) of RDF is explored for improving biochar quality by providing a better heating performance and pore development mechanism than conventional pyrolysis. Selecting appropriate additives and operating conditions are of great importance to produce high quality biochar in MACP of RDF.

In this study the heating performance of RDF mixed with 20 wt.% K_2CO_3 in the microwave reactor showed a high average heating rate (184 ℃/min) and biochar surface area (155.6 m^2/g) compared with previously reported data on conventional pyrolysis of RDF, whereas 30 wt.% K_2CO_3 showed the highest biochar surface area (285.6 m^2/g) among all catalyst cases, which indicated high dielectric properties and catalytic effect of K_2CO_3. The average heating rate of RDF mixed with K_3PO_4 was significantly increased by ~50% after adding bentonite and clinoptilolite, which proved the synergistic effect of dual catalysts on accelerating microwave absorption and heating rate. 20 wt.% K_2CO_3 + 10 wt.% bentonite was identified to be the best, at the optimum operation conditions of 1000 W microwave power input, 500 ℃ targeted pyrolysis temperature and 30 minutes

microwave radiation time. Statistical analysis revealed that the targeted pyrolysis temperature has the most significant effect on biochar surface area, compared to microwave radiation time and heating rate. The morphology of produced biochar varied between different catalysts and operating conditions. Biochar yield was around 15% due to the low carbon content and deep cracking of waste plastics in RDF. As functional groups responsible for chemisorption were not found from FTIR spectra, physisorption was believed to play an important role in MB adsorption.

The main goal of this project is to apply MACP to treat low quality municipal solid waste, which may provide an alternative for industrial disposal of solid waste. By combining microwave heating with catalysts in pyrolysis, RDF can be decomposed to biochar with high specific surface area, which favors its applications as solid sorbents. RDF derived biochar can be designed with the use of different catalysts based on specific targeted applications. For instance, K_2CO_3 is a suitable catalyst to enlarge and modify the pore structure of biochar for adsorption applications, while K_3PO_4 may be beneficial for plant growth and heavy metal adsorption in contaminated soil. Nevertheless, some limitations do exist in this study and need to be addressed in the future work:

1. Some heating performance and biochar quality data have a wide scattering, probably resulting from the heterogeneity of RDF but needing to be investigated. The composition of RDF varies between different regions as well, which means that the RDF feedstock in this study is only representative of the region of its origin. It is suggested to test more types of RDF samples from different regions.
2. A proper leaching model of biochar sample needs to be developed and used to investigate the potential beneficial and harmful elements in biochar to be leached out in soil environment.

3. The main catalysts used in this study are pure inorganic compounds which are not abundantly available. Other catalysts of low cost are worth investigated, such as the potassium containing minerals (potash). Meanwhile, the cost of catalysts can be further reduced by recycling catalysts. The performance of spent catalysts differs from fresh catalysts, because of fouling by coke formation. Recycling potential of catalysts should be then investigated.
4. Biochar yield from MACP of RDF was very low compared with woody biomass such as sawdust. Co-pyrolysis of RDF with carbon-rich feedstock may be explored if the overall biochar yield is desired.
5. The low solid yield indicates that large amounts of bio-oil and non-condensable gases are produced whose composition and heating value remain unexamined. Thus, the liquid and gas should be collected and analyzed in the future. It is highly desirable to improve bio-oil quality so as to make it upgraded easily in the downstream catalytic process into transportation fuels of higher value. The purification of combustible gases and removal of chloride originated from waste plastics are also of great topic for further investigation.
6. To scale-up this process, more considerations need to be taken into account, e.g. the combustion flue gas is expected to be used instead of pure N_2 to create the inert atmosphere in large scale pyrolysis process for economic reasons. The analysis of mass and energy balances can provide a systematic insight. As microwave pyrolysis has been demonstrated in some pilot and demonstrate plants to treat solid wastes, a techno-economic analysis could be helpful to assess the commercialization potential of the MACP of RDF.

Bibliography

Aguilar, C., García, R., Soto-Garrido, G., Arriagada, R., 2003. Catalytic wet air oxidation of aqueous ammonia with activated carbon. Appl. Catal. B Environ. 46, 229–237. https://doi.org/10.1016/S0926-3373(03)00229-7

Ahmad, M., Rajapaksha, A.U., Lim, J.E., Zhang, M., Bolan, N., Mohan, D., Vithanage, M., Lee, S.S., Ok, Y.S., 2014. Biochar as a sorbent for contaminant management in soil and water: A review. Chemosphere 99, 19–33. https://doi.org/10.1016/j.chemosphere.2013.10.071

Arshad, H., Sulaiman, S.A., Hussain, Z., Naz, Y., Basrawi, F., 2017. Microwave assisted pyrolysis of plastic waste for production of fuels: A review, in: MATEC Web of Conferences. https://doi.org/10.1051/matecconf/201713102005

Baçaoui, A., Yaacoubi, A., Dahbi, A., Bennouna, C., Phan Tan Luu, R., Maldonado-Hodar, F.J., Rivera-Utrilla, J., Moreno-Castilla, C., 2001. Optimization of conditions for the preparation of activated carbons from olive-waste cakes. Carbon N. Y. 39, 425–432. https://doi.org/10.1016/S0008-6223(00)00135-4

Bach, Q.-V., Tran, K.-Q., Skreiberg, Ø., Trinh, T.T., 2015. Effects of wet torrefaction on pyrolysis of woody biomass fuels. Energy 88, 443–456. https://doi.org/10.1016/J.ENERGY.2015.05.062

Bach, Q.V., Chen, W.H., 2017. Pyrolysis characteristics and kinetics of microalgae via thermogravimetric analysis (TGA): A state-of-the-art review. Bioresour. Technol. 246, 88–100. https://doi.org/10.1016/j.biortech.2017.06.087

Banks, S.W., Nowakowski, D.J., Bridgwater, A. V., 2016. Impact of Potassium and Phosphorus in Biomass on the Properties of Fast Pyrolysis Bio-oil. Energy and Fuels 30, 8009–8018. https://doi.org/10.1021/acs.energyfuels.6b01044

Barton, S.S., 1987. The adsorption of methylene blue by active carbon. Carbon N. Y. 25, 343–350. https://doi.org/10.1016/0008-6223(87)90005-4

Basu, P., 2013. Biomass Characteristics, in: Biomass Gasification, Pyrolysis and Torrefaction. https://doi.org/10.1016/b978-0-12-396488-5.00003-4

Belgiorno, V., De Feo, G., Della Rocca, C., Napoli, R.M.A., 2003. Energy from gasification of solid wastes. Waste Manag. 23, 1–15. https://doi.org/10.1016/S0956-053X(02)00149-6

Bolan, N., Kunhikrishnan, A., Thangarajan, R., Kumpiene, J., Park, J., Makino, T., Kirkham, M.B., Scheckel, K., 2014a. Remediation of heavy metal(loid)s contaminated soils – To mobilize or to immobilize? J. Hazard. Mater. 266, 141–166. https://doi.org/10.1016/J.JHAZMAT.2013.12.018

Bolan, N., Kunhikrishnan, A., Thangarajan, R., Kumpiene, J., Park, J., Makino, T., Kirkham, M.B., Scheckel, K., 2014b. Remediation of heavy metal(loid)s contaminated soils - To mobilize or to immobilize? J. Hazard. Mater. https://doi.org/10.1016/j.jhazmat.2013.12.018

Boonamnuayvitaya, V., Sae-Ung, S., Tanthapanichakoon, W., 2005. Preparation of activated carbons from coffee residue for the adsorption of formaldehyde. Sep. Purif. Technol. 42, 159–168. https://doi.org/10.1016/j.seppur.2004.07.007

Bridgwater, A. V., 2012. Review of fast pyrolysis of biomass and product upgrading. Biomass and Bioenergy 38, 68–94. https://doi.org/10.1016/j.biombioe.2011.01.048

Cao, Q., Huang, Z., Liu, S., Wu, Y., 2019. Potential of Punica granatum biochar to adsorb Cu(II) in soil. Sci. Rep. 9, 11116. https://doi.org/10.1038/s41598-019-46983-2

CCME, 2007. Canadian Soil Quality Guidelines for the Protection of Environmental and Human Health. https://doi.org/10.1177/004947559702700223

Cetin, E., Moghtaderi, B., Gupta, R., Wall, T.F., 2004. Influence of pyrolysis conditions on the

structure and gasification reactivity of biomass chars. Fuel 83, 2139–2150. https://doi.org/10.1016/j.fuel.2004.05.008

Cheng, F., Li, X., 2018. Preparation and application of biochar-based catalysts for biofuel production. Catalysts 8, 1–35. https://doi.org/10.3390/catal8090346

Chhabra, V., Shastri, Y., Bhattacharya, S., 2016. Kinetics of Pyrolysis of Mixed Municipal Solid Waste-A Review. Procedia Environ. Sci. 35, 513–527. https://doi.org/10.1016/j.proenv.2016.07.036

Chun, Y., Sheng, G., Chiou, G.T., Xing, B., 2004. Compositions and sorptive properties of crop residue-derived chars. Environ. Sci. Technol. 38, 4649–4655. https://doi.org/10.1021/es035034w

Cozzani, V., Nicolella, C., Petarca, L., Rovatti, M., Tognotti, L., 1995a. A Fundamental Study on Conventional Pyrolysis of a Refuse-Derived Fuel. Ind. Eng. Chem. Res. 34, 2006–2020. https://doi.org/10.1021/ie00045a010

Cozzani, V., Petarca, L., Tognotti, L., 1995b. Devolatilization and pyrolysis of refuse derived fuels: characterization and kinetic modelling by a thermogravimetric and calorimetric approach. Fuel 74, 903–912. https://doi.org/10.1016/0016-2361(94)00018-M

de Wild, P.J., Uil, H. den, Reith, J.H., Kiel, J.H.A., Heeres, H.J., 2009. Biomass valorisation by staged degasification: A new pyrolysis-based thermochemical conversion option to produce value-added chemicals from lignocellulosic biomass. J. Anal. Appl. Pyrolysis 85, 124–133. https://doi.org/10.1016/J.JAAP.2008.08.008

Deng, H., Li, G., Yang, H., Tang, Jiping, Tang, Jiangyun, 2010. Preparation of activated carbons from cotton stalk by microwave assisted KOH and K2CO3 activation. Chem. Eng. J. 163, 373–381. https://doi.org/10.1016/j.cej.2010.08.019

Dernovsek, O., Naeini, A., Preu, G., Wersing, W., Eberstein, M., Schiller, W.A., 2001. LTCC glass-ceramic composites for microwave application. J. Eur. Ceram. Soc. 21, 1693–1697. https://doi.org/10.1016/S0955-2219(01)00096-6

Di Blasi, C., Branca, C., Galgano, A., 2017. Influences of Potassium Hydroxyde on Rate and Thermicity of Wood Pyrolysis Reactions. Energy and Fuels 31, 6154–6162. https://doi.org/10.1021/acs.energyfuels.7b00536

Dmitry, S., 2011. Economics of Combined Power Plant and Pyrolysis Bio-Oil Production. Personnel.

Domínguez, A., Menéndez, J.A., Inguanzo, M., Pís, J.J., 2006. Production of bio-fuels by high temperature pyrolysis of sewage sludge using conventional and microwave heating. Bioresour. Technol. 97, 1185–1193. https://doi.org/10.1016/j.biortech.2005.05.011

Efika, E.C., Onwudili, J.A., Williams, P.T., 2015. Products from the high temperature pyrolysis of RDF at slow and rapid heating rates. J. Anal. Appl. Pyrolysis. https://doi.org/10.1016/j.jaap.2015.01.004

Ellis, 2018. World Bank: Global waste generation could increase 70% by 2050 [WWW Document].

Fahmi, A.H., Samsuri, A.W., Jol, H., Singh, D., 2018. Bioavailability and leaching of Cd and Pb from contaminated soil amended with different sizes of biochar. R. Soc. Open Sci. 5. https://doi.org/10.1098/rsos.181328

Farrell, M., Kuhn, T.K., Macdonald, L.M., Maddern, T.M., Murphy, D. V., Hall, P.A., Singh, B.P., Baumann, K., Krull, E.S., Baldock, J.A., 2013. Microbial utilisation of biochar-derived carbon. Sci. Total Environ. 465, 288–297. https://doi.org/10.1016/j.scitotenv.2013.03.090

Foo, K.Y., Hameed, B.H., 2012a. Factors affecting the carbon yield and adsorption capability of

the mangosteen peel activated carbon prepared by microwave assisted K 2CO 3 activation. Chem. Eng. J. 180, 66–74. https://doi.org/10.1016/j.cej.2011.11.002

Foo, K.Y., Hameed, B.H., 2012b. Porous structure and adsorptive properties of pineapple peel based activated carbons prepared via microwave assisted KOH and K2CO 3 activation. Microporous Mesoporous Mater. 148, 191–195. https://doi.org/10.1016/j.micromeso.2011.08.005

Foo, K.Y., Hameed, B.H., 2012c. Preparation, characterization and evaluation of adsorptive properties of orange peel based activated carbon via microwave induced K 2CO 3 activation. Bioresour. Technol. 104, 679–686. https://doi.org/10.1016/j.biortech.2011.10.005

Foo, K.Y., Hameed, B.H., 2011. Utilization of rice husks as a feedstock for preparation of activated carbon by microwave induced KOH and K 2CO 3 activation. Bioresour. Technol. 102, 9814–9817. https://doi.org/10.1016/j.biortech.2011.07.102

Fu, P., Hu, S., Sun, L., Xiang, J., Yang, T., Zhang, A., Zhang, J., 2009. Structural evolution of maize stalk/char particles during pyrolysis. Bioresour. Technol. 100, 4877–4883. https://doi.org/10.1016/J.BIORTECH.2009.05.009

Gates, W.P., Bouazza, A., Jock Churchman, G., 2009. Bentonite clay keeps pollutants at bay. Elements 5, 105–110. https://doi.org/10.2113/gselements.5.2.105

Grammelis, P., Basinas, P., Malliopoulou, A., Sakellaropoulos, G., 2009. Pyrolysis kinetics and combustion characteristics of waste recovered fuels. Fuel 88, 195–205. https://doi.org/10.1016/j.fuel.2008.02.002

Haeldermans, T., Claesen, J., Maggen, J., Carleer, R., Yperman, J., Adriaensens, P., Samyn, P., Vandamme, D., Cuypers, A., Vanreppelen, K., Schreurs, S., 2019. Microwave assisted and conventional pyrolysis of MDF – Characterization of the produced biochars. J. Anal. Appl.

Pyrolysis 138, 218–230. https://doi.org/10.1016/j.jaap.2018.12.027

He, M., Xiao, B., Liu, S., Hu, Z., Guo, X., Luo, S., Yang, F., 2010. Syngas production from pyrolysis of municipal solid waste (MSW) with dolomite as downstream catalysts. J. Anal. Appl. Pyrolysis 87, 181–187. https://doi.org/10.1016/j.jaap.2009.11.005

Huang, Y.F., Chiueh, P. Te, Lo, S.L., 2016. A review on microwave pyrolysis of lignocellulosic biomass. Sustain. Environ. Res. 26, 103–109. https://doi.org/10.1016/j.serj.2016.04.012

Hwang, H., Oh, S., Cho, T.S., Choi, I.G., Choi, J.W., 2013. Fast pyrolysis of potassium impregnated poplar wood and characterization of its influence on the formation as well as properties of pyrolytic products. Bioresour. Technol. 150, 359–366. https://doi.org/10.1016/j.biortech.2013.09.132

Ingole, P.M., Ranveer, A.C., Deshmukh, S.M., Deshmukh, S.K., 2016. Microwave Assisted Pyrolysis of Biomass: A Review. Int. J. Adv. Technol. Eng. Sci. 4, 78–84.

Inyang, M.I., Gao, B., Yao, Y., Xue, Y., Zimmerman, A., Mosa, A., Pullammanappallil, P., Ok, Y.S., Cao, X., 2016. A review of biochar as a low-cost adsorbent for aqueous heavy metal removal. Crit. Rev. Environ. Sci. Technol. 46, 406–433. https://doi.org/10.1080/10643389.2015.1096880

Jones, D.A., Lelyveld, T.P., Mavrofidis, S.D., Kingman, S.W., Miles, N.J., 2002. Microwave heating applications in environmental engineering - A review. Resour. Conserv. Recycl. 34, 75–90. https://doi.org/10.1016/S0921-3449(01)00088-X

Karayildirim, T., Yanik, J., Yuksel, M., Bockhorn, H., 2006. Characterisation of products from pyrolysis of waste sludges. Fuel 85, 1498–1508. https://doi.org/10.1016/j.fuel.2005.12.002

Khoeini, M., Bazgir, S., Tamizifar, M., Arzani, K., 2009. Investigation of the modification process and morphology of organosilane modified nanoclay. Ceram. - Silikaty 53.

Kucora, I., Paunjoric, P., Tolmac, J., Vulovic, M., Speight, J.G., Radovanović, L.Z., 2017. Coke formation in pyrolysis furnaces in the petrochemical industry. Pet. Sci. Technol. 35, 213–221. https://doi.org/10.1080/10916466.2016.1198810

Kumar, U., Maroufi, S., Rajarao, R., Mayyas, M., Mansuri, I., Joshi, R.K., Sahajwalla, V., 2017. Cleaner production of iron by using waste macadamia biomass as a carbon resource. J. Clean. Prod. 158, 218–224. https://doi.org/10.1016/j.jclepro.2017.04.115

Li, J., Dai, J., Liu, G., Zhang, H., Gao, Z., Fu, J., He, Y., Huang, Y., 2016. Biochar from microwave pyrolysis of biomass: A review. Biomass and Bioenergy. https://doi.org/10.1016/j.biombioe.2016.09.010

Liew, R.K., Nam, W.L., Chong, M.Y., Phang, X.Y., Su, M.H., Yek, P.N.Y., Ma, N.L., Cheng, C.K., Chong, C.T., Lam, S.S., 2018. Oil palm waste: An abundant and promising feedstock for microwave pyrolysis conversion into good quality biochar with potential multi-applications. Process Saf. Environ. Prot. 115, 57–69. https://doi.org/10.1016/j.psep.2017.10.005

Liu, W.J., Jiang, H., Yu, H.Q., 2015. Development of Biochar-Based Functional Materials: Toward a Sustainable Platform Carbon Material. Chem. Rev. 115, 12251–12285. https://doi.org/10.1021/acs.chemrev.5b00195

Liu, X., Bi, X.T., Liu, C., Liu, Y., 2012. Performance of Fe/AC catalyst prepared from demineralized pine bark particles in a microwave reactor. Chem. Eng. J. 193–194, 187–195. https://doi.org/10.1016/j.cej.2012.04.039

Longo, S., Cellura, M., Girardi, P., 2020. Life Cycle Assessment of electricity production from refuse derived fuel: A case study in Italy. Sci. Total Environ. 738, 139719. https://doi.org/10.1016/j.scitotenv.2020.139719

Lu, G.Q., 1994. Evolution of pore structure of high-ash char during activation. Fuel 73, 145–147. https://doi.org/10.1016/0016-2361(94)90203-8

Lu, Q., Zhang, Z., Wang, X., Guo, H., Cui, M., Yang, Y., 2018. Catalytic Fast Pyrolysis of Biomass Impregnated with Potassium Phosphate in a Hydrogen Atmosphere for the Production of Phenol and Activated Carbon. Front. Chem. 6, 1–10. https://doi.org/10.3389/fchem.2018.00032

Luque, R., Menéndez, J.A., Arenillas, A., Cot, J., 2012. Microwave-assisted pyrolysis of biomass feedstocks: The way forward? Energy Environ. Sci. 5, 5481–5488. https://doi.org/10.1039/c1ee02450g

Manyà, J.J., García-Ceballos, F., Azuara, M., Latorre, N., Royo, C., 2015. Pyrolysis and char reactivity of a poor-quality refuse-derived fuel (RDF) from municipal solid waste. Fuel Process. Technol. 140, 276–284. https://doi.org/10.1016/j.fuproc.2015.09.014

McKee, D.W., 1983. Mechanisms of the alkali metal catalysed gasification of carbon. Fuel 62, 170–175. https://doi.org/10.1016/0016-2361(83)90192-8

Menéndez, J.A., Arenillas, A., Fidalgo, B., Fernández, Y., Zubizarreta, L., Calvo, E.G., Bermúdez, J.M., 2010. Microwave heating processes involving carbon materials. Fuel Process. Technol. 91, 1–8. https://doi.org/10.1016/j.fuproc.2009.08.021

Menéndez, J.A., Domínguez, A., Fernández, Y., Pis, J.J., 2007. Evidence of self-gasification during the microwave-induced pyrolysis of coffee hulls. Energy and Fuels 21, 373–378. https://doi.org/10.1021/ef060331i

Metaxas, A.C., Meredith, R.J., 2011. Dielectric loss. Ind. Microw. Heat. 5–25. https://doi.org/10.1049/pbpo004e_ch2

Miandad, R., Barakat, M.A., Rehan, M., Aburiazaiza, A.S., Ismail, I.M.I., Nizami, A.S., 2017.

Plastic waste to liquid oil through catalytic pyrolysis using natural and synthetic zeolite catalysts. Waste Manag. 69, 66–78. https://doi.org/10.1016/j.wasman.2017.08.032

Miretzky, P., Fernandez-Cirelli, A., 2008. Phosphates for Pb immobilization in soils: A review. Environ. Chem. Lett. 6, 121–133. https://doi.org/10.1007/s10311-007-0133-y

Miura, M., Kaga, H., Sakurai, A., Kakuchi, T., Takahashi, K., 2004. Rapid pyrolysis of wood block by microwave heating. J. Anal. Appl. Pyrolysis 71, 187–199. https://doi.org/10.1016/S0165-2370(03)00087-1

Mohamed, B.A., 2018. Microwave-assisted catalytic pyrolysis of biomass for improving bio-oil and biochar properties. The University of British Columbia, Vancouver, Canada.

Mohamed, B.A., Ellis, N., Kim, C.S., Bi, X., 2019. Microwave-assisted catalytic biomass pyrolysis: Effects of catalyst mixtures. Appl. Catal. B Environ. 253, 226–234. https://doi.org/10.1016/j.apcatb.2019.04.058

Mohamed, B.A., Ellis, N., Kim, C.S., Bi, X., Emam, A.E.R., 2016a. Engineered biochar from microwave-assisted catalytic pyrolysis of switchgrass for increasing water-holding capacity and fertility of sandy soil. Sci. Total Environ. 566–567, 387–397. https://doi.org/10.1016/j.scitotenv.2016.04.169

Mohamed, B.A., Kim, C.S., Ellis, N., Bi, X., 2016b. Microwave-assisted catalytic pyrolysis of switchgrass for improving bio-oil and biochar properties. Bioresour. Technol. 201, 121–132. https://doi.org/10.1016/j.biortech.2015.10.096

Mullen, C.A., Boateng, A.A., Goldberg, N.M., Lima, I.M., Laird, D.A., Hicks, K.B., 2010. Bio-oil and bio-char production from corn cobs and stover by fast pyrolysis. Biomass and Bioenergy 34, 67–74. https://doi.org/10.1016/j.biombioe.2009.09.012

Muradov, N., Fidalgo, B., Gujar, A.C., Garceau, N., T-Raissi, A., 2012. Production and

characterization of Lemna minor bio-char and its catalytic application for biogas reforming. Biomass and Bioenergy 42, 123–131. https://doi.org/10.1016/j.biombioe.2012.03.003

Mushtaq, F., Mat, R., Ani, F.N., 2014. A review on microwave assisted pyrolysis of coal and biomass for fuel production. Renew. Sustain. Energy Rev. https://doi.org/10.1016/j.rser.2014.07.073

Nomanbhay, S., Salman, B., Hussain, R., Ong, M.Y., 2017. Microwave pyrolysis of lignocellulosic biomass—a contribution to power Africa. Energy. Sustain. Soc. 7. https://doi.org/10.1186/s13705-017-0126-z

Nowicki, P., Kazmierczak-Razna, J., Pietrzak, R., 2016. Physicochemical and adsorption properties of carbonaceous sorbents prepared by activation of tropical fruit skins with potassium carbonate. Mater. Des. 90, 579–585. https://doi.org/10.1016/j.matdes.2015.11.004

Okman, I., Karagöz, S., Tay, T., Erdem, M., 2014. Activated carbons from grape seeds by chemical activation with potassium carbonate and potassium hydroxide. Appl. Surf. Sci. 293, 138–142. https://doi.org/10.1016/j.apsusc.2013.12.117

Osborne, L.R., Baker, L.L., Strawn, D.G., 2015. Lead immobilization and phosphorus availability in phosphate-amended, mine-contaminated soils. J. Environ. Qual. 44, 183–190. https://doi.org/10.2134/jeq2014.07.0323

Ozkan, A., Banar, M., 2010. Refuse derived fuel (RDF) utilization in cement industry by using Analytic Network Process (ANP). Chem. Eng. Trans. 21, 769–774. https://doi.org/10.3303/CET1021129

Park, D.K., Kim, S.D., Lee, S.H., Lee, J.G., 2010. Co-pyrolysis characteristics of sawdust and coal blend in TGA and a fixed bed reactor. Bioresour. Technol. 101, 6151–6156. https://doi.org/10.1016/j.biortech.2010.02.087

Park, D.W., Hwang, E.Y., Kim, J.R., Choi, J.K., Kim, Y.A., Woo, H.C., 1999. Catalytic degradation of polyethylene over solid acid catalysts. Polym. Degrad. Stab. 65, 193–198. https://doi.org/10.1016/S0141-3910(99)00004-X

Pelekani, C., Snoeyink, V.L., 1999. Competitive adsorption in natural water: Role of activated carbon pore size. Water Res. 33, 1209–1219. https://doi.org/10.1016/S0043-1354(98)00329-7

Puga, A.P., Abreu, C.A., Melo, L.C.A., Beesley, L., 2015. Biochar application to a contaminated soil reduces the availability and plant uptake of zinc, lead and cadmium. J. Environ. Manage. 159, 86–93. https://doi.org/10.1016/j.jenvman.2015.05.036

Pütun, E., Uzun, B.B., Putün, A.E., 2009. Rapid pyrolysis of olive residue. 2. Effect of catalytic upgrading of pyrolysis vapors in a two-stage fixed-bed reactor. Energy and Fuels 23, 2248–2258. https://doi.org/10.1021/ef800978m

Schwenke, A.M., Hoeppener, S., Schubert, U.S., 2015. Synthesis and Modification of Carbon Nanomaterials utilizing Microwave Heating. Adv. Mater. 27, 4113–4141. https://doi.org/10.1002/adma.201500472

Seo, M.W., Kim, S.D., Lee, S.H., Lee, J.G., 2010. Pyrolysis characteristics of coal and RDF blends in non-isothermal and isothermal conditions. J. Anal. Appl. Pyrolysis 88, 160–167. https://doi.org/10.1016/j.jaap.2010.03.010

Shang, H., Lu, R.R., Shang, L., Zhang, W.H., 2015. Effect of additives on the microwave-assisted pyrolysis of sawdust. Fuel Process. Technol. 131, 167–174. https://doi.org/10.1016/j.fuproc.2014.11.025

Silva, R.B., Martins-Dias, S., Arnal, C., Alzueta, M.U., Costa, M., 2015. Pyrolysis and char characterization of refuse-derived fuel components. Energy and Fuels 29, 1997–2005.

https://doi.org/10.1021/ef502011f

Singh, R.K., Ruj, B., Sadhukhan, A.K., Gupta, P., 2019. Thermal degradation of waste plastics under non-sweeping atmosphere: Part 1: Effect of temperature, product optimization, and degradation mechanism. J. Environ. Manage. 239, 395–406. https://doi.org/10.1016/j.jenvman.2019.03.067

Singh, S., Wu, C., Williams, P.T., 2012. Pyrolysis of waste materials using TGA-MS and TGA-FTIR as complementary characterisation techniques. J. Anal. Appl. Pyrolysis 94, 99–107. https://doi.org/10.1016/J.JAAP.2011.11.011

Spokas, K.A., Cantrell, K.B., Novak, J.M., Archer, D.W., Ippolito, J.A., Collins, H.P., Boateng, A.A., Lima, I.M., Lamb, M.C., McAloon, A.J., Lentz, R.D., Nichols, K.A., 2012. Biochar: A synthesis of its agronomic impact beyond carbon sequestration. J. Environ. Qual. 41, 973–989. https://doi.org/10.2134/jeq2011.0069

Sulman, M., Kosivtsov, Y., Sulman, E., Alfyorov, V., Lugovoy, Y., Molchanov, V., Tyamina, I., Misnikov, O., Afanasjev, A., Kumar, N., Murzin, D., 2009. Influence of aluminosilicate materials on the peat low-temperature pyrolysis and gas formation. Chem. Eng. J. 154, 355–360. https://doi.org/10.1016/j.cej.2009.04.001

Tay, T., Ucar, S., Karagöz, S., 2009. Preparation and characterization of activated carbon from waste biomass. J. Hazard. Mater. 165, 481–485. https://doi.org/10.1016/j.jhazmat.2008.10.011

Trendewicz, A., Evans, R., Dutta, A., Sykes, R., Carpenter, D., Braun, R., 2015. Evaluating the effect of potassium on cellulose pyrolysis reaction kinetics. Biomass and Bioenergy 74, 15–25. https://doi.org/10.1016/j.biombioe.2015.01.001

Tripathi, M., Sahu, J.N., Ganesan, P., 2016. Effect of process parameters on production of biochar

from biomass waste through pyrolysis: A review. Renew. Sustain. Energy Rev. https://doi.org/10.1016/j.rser.2015.10.122

Veksha, A., McLaughlin, H., Layzell, D.B., Hill, J.M., 2014. Pyrolysis of wood to biochar: Increasing yield while maintaining microporosity. Bioresour. Technol. 153, 173–179. https://doi.org/10.1016/j.biortech.2013.11.082

Villota, E.M., Lei, H., Qian, M., Yang, Z., Villota, S.M.A., Zhang, Y., Yadavalli, G., 2018. Optimizing Microwave-Assisted Pyrolysis of Phosphoric Acid-Activated Biomass: Impact of Concentration on Heating Rate and Carbonization Time. ACS Sustain. Chem. Eng. 6, 1318–1326. https://doi.org/10.1021/acssuschemeng.7b03669

Wang, C., Wang, W., Lin, L., Zhang, F., Zhang, R., Sun, J., Song, Z., Mao, Y., Zhao, X., 2020. A stepwise microwave synergistic pyrolysis approach to produce sludge-based biochars: Feasibility study simulated by laboratory experiments. Fuel 272, 117628. https://doi.org/10.1016/j.fuel.2020.117628

Wang, H., Xia, W., Lu, P., 2017. Study on adsorption characteristics of biochar on heavy metals in soil. Korean J. Chem. Eng. 34, 1867–1873. https://doi.org/10.1007/s11814-017-0048-7

Xiao, X., Chen, B., Chen, Z., Zhu, L., Schnoor, J.L., 2018. Insight into Multiple and Multilevel Structures of Biochars and Their Potential Environmental Applications: A Critical Review. Environ. Sci. Technol. 52, 5027–5047. https://doi.org/10.1021/acs.est.7b06487

Yang, H., Yan, R., Chen, H., Lee, D.H., Zheng, C., 2007. Characteristics of hemicellulose, cellulose and lignin pyrolysis. Fuel 86, 1781–1788. https://doi.org/10.1016/J.FUEL.2006.12.013

Yao, Y., Gao, B., Zhang, M., Inyang, M., Zimmerman, A.R., 2012. Effect of biochar amendment on sorption and leaching of nitrate, ammonium, and phosphate in a sandy soil. Chemosphere

89, 1467–1471. https://doi.org/10.1016/j.chemosphere.2012.06.002

Yin, C., 2012. Microwave-assisted pyrolysis of biomass for liquid biofuels production. Bioresour. Technol. https://doi.org/10.1016/j.biortech.2012.06.016

Zhang, H., Ma, Y., Shao, S., Xiao, R., 2017. The effects of potassium on distributions of bio-oils obtained from fast pyrolysis of agricultural and forest biomass in a fluidized bed. Appl. Energy 208, 867–877. https://doi.org/10.1016/j.apenergy.2017.09.062

Zhang, J., Liu, J., Liu, R., 2015. Effects of pyrolysis temperature and heating time on biochar obtained from the pyrolysis of straw and lignosulfonate. Bioresour. Technol. 176, 288–291. https://doi.org/10.1016/J.BIORTECH.2014.11.011

Zhang, R., Li, L., Tong, D., Hu, C., 2016. Microwave-enhanced pyrolysis of natural algae from water blooms. Bioresour. Technol. 212, 311–317. https://doi.org/10.1016/j.biortech.2016.04.053

Zhao, B., O'Connor, D., Zhang, J., Peng, T., Shen, Z., Tsang, D.C.W., Hou, D., 2018. Effect of pyrolysis temperature, heating rate, and residence time on rapeseed stem derived biochar. J. Clean. Prod. 174, 977–987. https://doi.org/10.1016/j.jclepro.2017.11.013

Zhao, C., Jiang, E., Chen, A., 2017. Volatile production from pyrolysis of cellulose, hemicellulose and lignin. J. Energy Inst. 90, 902–913. https://doi.org/10.1016/j.joei.2016.08.004

Zhao, X., Wang, W., Liu, H., Ma, C., Song, Z., 2014. Microwave pyrolysis of wheat straw: Product distribution and generation mechanism. Bioresour. Technol. 158, 278–285. https://doi.org/10.1016/j.biortech.2014.01.094

Zhuang, X., Zhan, H., Song, Y., He, C., Huang, Y., Yin, X., Wu, C., 2019. Insights into the evolution of chemical structures in lignocellulose and non-lignocellulose biowastes during hydrothermal carbonization (HTC). Fuel 236, 960–974.

https://doi.org/10.1016/j.fuel.2018.09.019

Zlotorzynski, A., 1995. The Application of Microwave Radiation to Analytical and Environmental Chemistry. Crit. Rev. Anal. Chem. 25, 43–76. https://doi.org/10.1080/10408349508050557

Appendices

Appendix A Heating performance of RDF mixed with bentonite or clinoptilolite in MACP

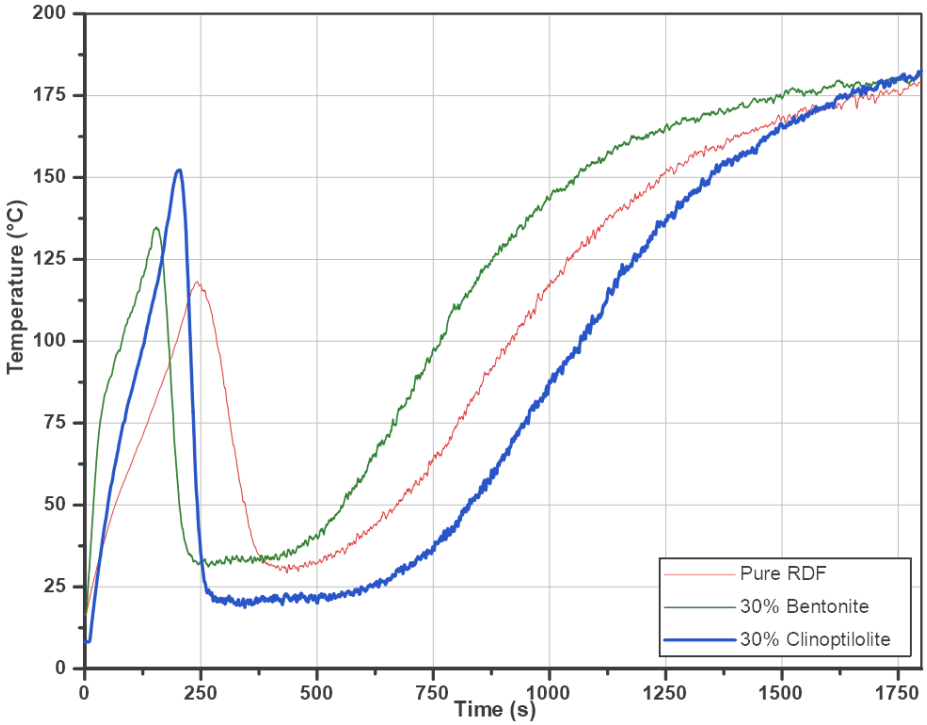

Figure A.1 Heating performance of pure RDF and RDF mixed with 30 wt.% bentonite or clinoptilolite in MACP.

Appendix B Stretching and functional groups in FTIR

Table B.1 Functional groups and chemical bonds under related wavenumbers in FTIR.

Wavenumber (cm^{-1})	Vibration type	Functionality groups
3640-3610	O-H stretching	Not bonded hydroxyl groups
3600-3200	O-H stretching	Bonded hydroxyl groups and water
3500-3300	N-H stretching	Amide II
3080	C-H stretching	Aromatic hydrogen
2925	C-H stretching	Asymmetric R_2CH_2
2885	C-H stretching	Symmetric RCH_3
2855	C-H stretching	Symmetric R_2CH_2
1720-1650	C=O stretching	Saturated ketone carbonyl, Amide I, carboxylates
1650	C=C stretching	Olefins conjugated with aromatic ring or double bonds
1580-1540	N-H bending	Amide II
1600, 1530, 1450	C-C stretching	Aromatic structure
1575, 1545	C-C stretching	Polycyclic aromatic structure
1384	N-O stretching	Nitrate in solid waste samples
1395,1325	$-CH_3$ stretching	Symmetric $-CH_3$-Ar, R
1295, 1275	C-O-C stretching	Cyclic ethers, aryl ethers
1265-1240	C-N stretching	Amide III
1245, 1225	C-O-C stretching	Aliphatic ethers
1140,1120	C-O stretching	C-O in hydroxyl group
1075	C-O stretching	C-O in alcohols
955-915	-O-H bending	Carboxyl groups

References (Aguilar et al., 2003; Domínguez et al., 2006; Fu et al., 2009; Haeldermans et al., 2019; Liu et al., 2012).

Appendix C Methylene blue adsorption test

Table C.1 MB adsorption of biochar samples produced from different catalysts in MACP of RDF, sawdust (SD) and conventional heating of RDF (CH) (solid to liquid ratio: 0.01 g:20 ml, concentration: 7.5*E-5 M).

Biochar type	MB Removal efficiency (%)	Surface area (m^2/g)	Micropore volume (cm^3/g)	Mesopore volume (cm^3/g)
30%KC	31.02	285.6	0.070	0.145
20%KC	10.14	156.0	0.037	0.079
20%KP	8.01	66.4	-	0.093
20%KC+10%B	6.02	205.8	0.060	0.083
20%KP+10%C	6.31	54.3	-	0.087
(CH) 20%KC+10%B	3.13	60.2	-	0.077
(SD) 20%KC+10%B	14.56	357.9	0.106	0.122

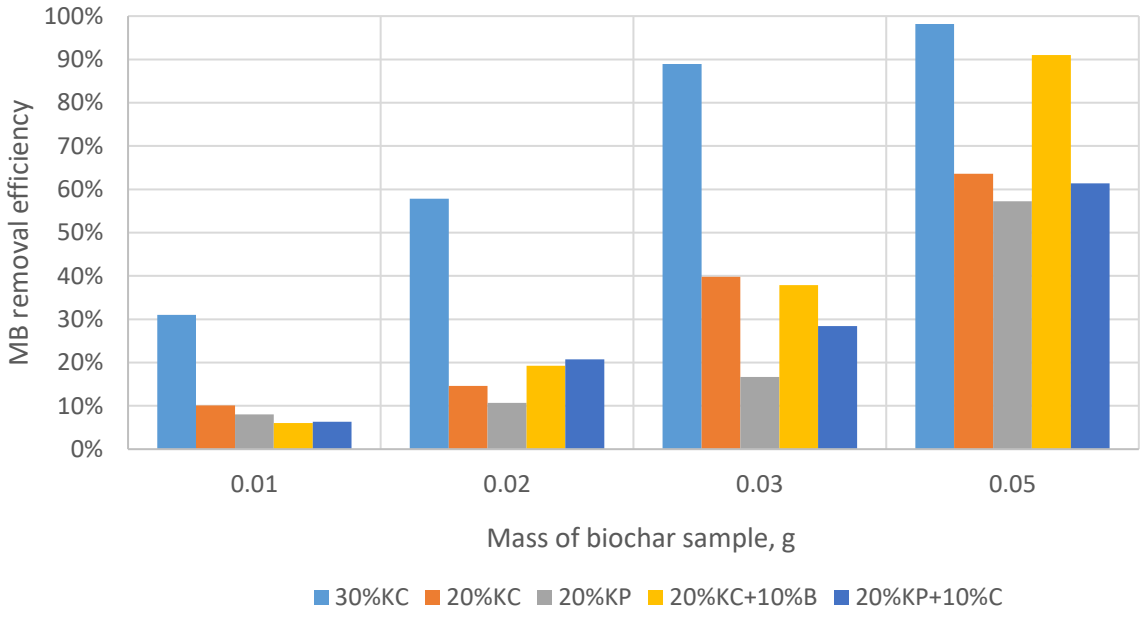

Figure C.1 MB adsorption of biochar sample produced from different catalysts in MACP of RDF at different solid to liquid ratios (MB solution volume: 20 ml, concentration: 7.5*E-5 M).

* Due to the research curtailment brought by COVID-19, these tests have not been repeated.

Appendix D Batch leaching test

Table D.1 Metal contents (ppm) of original biochar sample produced with different catalysts in MACP, RDF and RDF ash sample in leachates.

Sample	Cd	Cr	Pb	Fe	Zn	Ni	Cu
20KP	0.05	0.08	0.06	1.63	0.62	0.05	0.05
20KP+10C	0.06	0.06	0.05	1.67	0.20	0.06	0.04
20KC	0.07	0.05	0.07	0.19	0.06	0.05	0.04
20KC+10B	0.05	0.05	0.05	0.25	0.06	0.04	0.05
RDF	0.06	0.05	0.04	0.07	0.09	0.05	0.04
RDF burned ash	0.05	0.05	0.05	0.05	0.05	0.05	0.04
Hazardous waste*	1.0*	5.0*	5.0*				

* Regulated toxicity levels in Toxicity Characteristic Leaching Procedure (TCLP) from US EPA Hazardous Waste Identification (40 CFR Parts 261).

Appendix E Sample of descriptive and multiple comparisons of ANOVA

Table E.1 ANOVA descriptive table of surface area of biochar produced under different targeted pyrolysis temperature.

Temp. (℃)	N	Mean	Standard Deviation	Standard Error	Lower Bound*	Upper Bound*	Minimum	Maximum
400	3	135.8	24.9	14.4	74.0	197.6	108.5	157.0
450	3	186.9	21.4	12.4	133.6	240.2	170.2	211.1
500	3	265.0	5.9	3.4	250.2	279.7	260.3	271.6
550	3	225.1	16.9	9.8	183.1	267.2	206.1	238.4
Total	12	203.2	52.3	15.1	170.0	236.4	108.5	271.6

* 95% confidence interval for mean.

Table E.2 ANOVA multiple comparisons of surface area of biochar produced under different targeted pyrolysis temperature.

Temperature (℃)		Mean Difference	Standard Error	Sig. (p)	Lower Bound*	Upper Bound*
400	450	-51.1	15.3	0.041	-100.0	-2.2
	500	-129.2	15.3	0.000	-178.1	-80.2
	550	-89.3	15.3	0.002	-138.2	-40.4
450	400	51.1	15.3	0.041	2.2	100.0
	500	-78.1	15.3	0.004	-127.0	-29.2
	550	-38.2	15.3	0.134	-87.1	10.7
500	400	129.2	15.3	0.000	80.2	178.1
	450	78.1	15.3	0.004	29.2	127.0
	550	39.8	15.3	0.116	-9.1	88.7
550	400	89.3	15.3	0.002	40.4	138.2
	450	38.2	15.3	0.134	-10.7	87.1
	500	-39.8	15.3	0.116	-88.7	9.1

* 95% confidence interval.